Measurement of the fourth cumulant of photo-assisted noise in a tunnel junction in the classical regime.

Mesure du quatrième cumulant du bruit photo-assisté dans une jonction tunnel en régime classique.

par

Fatou Bintou SANE

au département de physique
en vue de l'obtention du grade de maître ès sciences (M.Sc.)

FACULTÉ DES SCIENCES
UNIVERSITÉ DE SHERBROOKE

Sherbrooke, Québec, Canada, le 19 Décembre 2013

Le 19 Décembre 2013

le jury a accepté le mémoire de Madame Fatou Bintou SANE dans sa version finale.

Membres du jury

Professeur Bertrand REULET
Directeur de recherche
Département de physique

Professeur Alexandre BLAIS
Membre interne
Département de physique

Professeur Michel PIORO-LADRIÈRE
Président-rapporteur
Département de physique

À ceux qui me reconnaitront.

Résumé

Les statistiques des fluctuations de courant dans un échantillon mésoscopique sous irradiation n'ont jamais été explorées au-delà de la variance et du troisième moment. Nous rapportons la première mesure du quatrième cumulant de bruit dans une jonction tunnel dans le régime classique (c'est-à-dire $k_B T \gg hf$) en présence d'un courant continu et d'une excitation micro-onde en utilisant deux méthodes. Tout d'abord, nous avons étudié la corrélation entre les fluctuations de puissance à deux fréquences, $f_1 = 4,5$ GHz et $f_2 = 7,15$ GHz. Cette corrélation existe seulement pour certaines fréquences d'excitation. Nous avons également effectué une mesure directe des statistiques en numérisant le bruit à grande vitesse après conversion vers les basses fréquences. Les résultats obtenus à partir de ces expériences sont en très bon accord avec les prédictions théoriques de la dynamique de bruit. En terme de photons, le quatrième cumulant correspond à une corrélation entre les photons de différentes fréquences.

Mots clés: quatrième cumulant, bruit photo-assisté.

Abstract

The statistics of current fluctuations in a mesoscopic sample under irradiation has never been explored beyond the variance and third moment. We report the first measurement of the fourth cumulant of noise in a tunnel junction in the classical regime (*i.e.* $k_B\ T \gg hf$) in the presence of a d.c and microwave excitation, using two methods. First, we have investigated the correlation between the power fluctuations at two frequencies, f_1 = 4.5 GHz and f_2 = 7.15 GHz. This correlation exists only for certain excitation frequencies. We have also performed a direct measurement of the statistics by digitizing the noise at high speed after down conversion. The results obtained from these experiments are in very good agreement with the theoretical predictions of noise dynamics. In terms of photons, the fourth cumulant corresponds to a correlation between photons of different frequencies.

Keyswords: fourth cumulant, photo-assisted noise.

Acknowledgements

I would like to thank my supervisor Prof. Bertrand Reulet for his support during this dissertation, for his patience, motivation and immense knowledge in Mesoscopic physics. He was available to answer any questions whether they were theoretical or experimental. I think, I have bored him a lot with my questions which were sometimes "stupid" or "evident" but he answered them as if they were very important. I could not have had a better supervisor than him.

My respects to Christian Lupien for his immense computing skills. He was not only an expert in python, but at same time the "technician" and the "Librarian" because he knows the documentation of almost every electronic device in our lab. In addition to that, he has the abilities and the facility to make them interact using python. Without him, our experiments would have taken a much longer time.

Having studied Theoretical Physics, I had never imagined being able to do a transfer of liquid helium in a cryostat for the cooling process, or being able to connect the electronic devices together, or more it would has been possible for me to do an experiment alone, etc. If I have acquired these expertises it is because of my colleague Jean-charles Forgues with whom I have learned many things and took the first part of the measurement of noise power correlation G_2.

Thanks to Simon Blanchard who has provided us a code C++ for statistic analysis. His code was very useful for the measurement of the fourth cumulant of current noise which I have taken alone since I was confident and autonomous. Thank to Lafe Spietz for his good sample "tunnel junction".

My sincere gratitudes to the other members of Bertrand's lab, my officemates: Karl Thibault, Kevin Spahr and Gabriel Gasse without forgetting my friend, classmate and "wire-bonding teacher": Jean-Olivier Simoneau (JO) for the discussions we had, for their suggestions and encouragements. I have really enjoyed these two years of work with them.

Many thanks also to Gabriel Laliberté for his technical support, to my lecturers for their excellent courses, to the EPIQ team particularly to Dr.Winton Brown for his kindness he was willing to correct my dissertation.

Dominique Parisé and Marc Leclair were also fantastic and encouraging.

I thank my committee members: Michel Pioro-Ladrière the chairman, Alexandre Blais and Bertrand Reulet my supervisor.

I can not finish without thanking my "ex-classmate" from Senegal and in Italy (ICTP): Jean Paul Latyr Faye with whom I have shared five good years of studies. I am indebted to Noelle for her warm welcome in Sherbrooke, for sending me to the dentist and for sharing her good dinner with us. May God bless her family.

Thanks to the Université de Sherbrooke in particular the department of Physics and Canada Excellence Research Chairs for the financial support. Thank also to the staff: Lise Charbonneau, Sylvie Perreault, Gilbert Vachon, Patrick Vachon ...

I also wish to express my deep gratitudes to Josiane Pafeng Tchuindjang my best friend, "ex-classmate" and "ex-officemate" at ICTP. She has really boosted my morale when I have needed most it. Without her, I would have never accepted to do again a Master in Physics. She was so far in Wyoming doing her PhD but so near to me when I was depressing and I going to be mad.

Last but not the least, I would like to thank my family: my Mom and Dad for giving a chance to study, to Sylvia Yaptieu and all friends.

I dedicate this work to uncle Ibrahima Badji, my brothers and cousins who believed on my success but, unfortunately, will not see it. Salute, peace and rest to their souls amine ya rabi amine.

Contents

List of Tables

List of Figures

Introduction

The study of second-order and higher noise cumulants in non-equilibrium systems is a powerful way to probe the statistics of current fluctuations [1, 2]. These quantities are commonly used in physics, engineering, chemistry ..., because many of the systems of interest contain a large number of particles, even when they have small size. Moreover, the random distribution of these charged particles is such that physical phenomena are not likely to recur with certainty in the measurements although static parameters are set. In other words, each experiment gives different results compared the previous ones. In such cases, only a statistical description may be promising for understanding these phenomena [3, 4].

In addition, experiments that have been done on many samples. In particular the measurement of shot noise on mesoscopic[1] phase coherent conductors have revealed additional information on the quantum's mechanism [5,6]. Indeed, because these conductors whose lengths L are bounded by the deBroglie wavelength of electron L_B and the phase coherence length L_ϕ[2] ($L_B \ll L < L_\phi$) are so small that the quantum nature of electrons dominates the transport properties. Most importantly, the phase coherence over distance larger than the dimensions of the conductors leads to results such as universal conductance fluctuations, weak localization and Aharonov Bohm effects [7].

These effects, which cannot be described by the classical conductance relating the net current to the supplied voltage, have been highlighted long time ago [8, 9] and more extended by Büttiker [10] in his calculations of correlation spectra of the current and flux. Using the exchange property of indistinguishable particles, it was possible to show the existence of an intrinsic relationship between correlation spectra of the current and the scattering matrix of a conductor. Hence, the number of experiments and theories

[1] mesoscopic physics is a field of condensed matter physics in between microscopic and macroscopic physics.

[2] L_ϕ distance beyond which an electron loses the memory of its phase.

have not ceased to grow during the past 20 years [6,11].

Nowadays, more attention has been paid to the photo-assisted noise (PAN) [3,12–14] since it permits not only to investigate the phase and amplitude modulation of the current fluctuations under d.c and a.c bias but can also be useful for the reconstruction of the energy band structure of the composite materials [15].

More recently, Gabelli and Reulet [**?**,16] have established relations between the correlator $\langle i(f)i(nf_0-f)\rangle$ describing noise dynamics at arbitrary frequencies f and excitation f_0, noise susceptibility[3] and PAN. Their studies have revealed that the environmental feedback and higher order cumulants of noise can be well understood from the noise susceptibility. However, the latter remains less studied.

In the present work, we would like to explore the statistic of electronic transport in presence of a.c excitation. To do that, we have measured the fourth cumulant of PAN in a tunnel junction in the classical regime, *i.e.* $k_BT \gg hf$ this in order to prove the non-Gaussian distribution of PAN.

We first performed the measurement of the cross-correlation between power fluctuations of noise, $G_2 = \langle P_1P_2\rangle - \langle P_1\rangle\langle P_2\rangle$, emanating from two independent filters centered at $f_1 = 4.5$ GHz and $f_2 = 7.15$ GHz. Our experiment setup is similar to that used for microwave photon correlation [17]. The source of microwave light here is a tunnel junction; that is d.c and a.c voltage biased (V_{dc} and V_{ac} respectively) at an excitation frequency f_0. We have observed that G_2 is non zero (*i.e.* that P_1 and P_2 are correlated) at some specific excitation frequencies, *i.e.* when $f_0 = f_1 + f_2$, $f_1 - f_2$ and $(f_2 - f_1)/2$. At these frequencies, we have measured G_2 as a function of the d.c bias voltage for different amplitudes of V_{ac} and have noticed that G_2 displayed similar behavior when $f_0 = f_2 \pm f_1$.

We have shown that G_2 is related to the fourth cumulant $C_4(f_1, f_2, 0)$. To prove this, we have measured C_4 by direct digitization of scanned noise. The data obtained with both methods is in very good agreement with theoretical predictions.

In what follows, we will attempt to detail the various procedures that have minnows to obtain these results. Before that, in the first chapter we begin to recall the basic notions of statistics that are useful for the understanding of this work. The second chapter will give an introduction into the concept of fluctuation (noise), its origins and characteristics for a mesoscopic conductor. Of particular interest is a tunnel junction for which the properties such as the spectral density of current fluctuations, the photo-assisted noise and the noise susceptibility are discussed as well as the electrical current and

[3] describing the response of noise under small variation of ac excitation

conductance. The third chapter will concern the theory developed to explain the fourth cumulant from the cross-correlation of power fluctuations. While the fourth chapter will introduce the preliminary steps and experiment. In the last chapter, we present the main results together with analysis and discussions before concluding.

Author contributions. I performed the measurements of G_2 with Jean-charles Forgues (J-C. F.) because at the beginning of this project my backgrounds were only theoretical physics. So, it was much easier for me to understand the theory, to calculate power supplied and recognize the symbols of the electronic devices drawn on paper but I had ever seen them in reality. Therefore, I think for the safety of the lab Bertrand had decided that J-C. F. and me will take the measurements together since he was an expert. Therefore, we did the cooling process together, he taught me how to connect devices and then I realized our experimental setup. Whenever, I added or removed, tested a device, wrote a script for data acquisition he had to approve it before we started the acquisition. I have also written a script in Mathematica to theoretically simulate the expected curves for G_2. After that, I performed the measurements of the fourth cumulant of current C_4 alone (second part of this project) and with help of my supervisor (Bertrand) established the theory developed in the third chapter3.

Simon Blanchard designed and implemented the code to digitize the correlator G_2. Lafe Spietz fabricated the samples. Christian Lupien programmed the codes to control all the components of the experimental setup. He also rectified the code written by Simon Blanchard in order to determine the histograms. This project was conceived and supervised by Bertrand.

P.S. In the following, the author's "we" is used to denote scientific detachment from the research process. The results obtained in the first part of this project have been subject of an article published in Scientific Reports [13] whose title is "Noise Intensity-Intensity Correlations and the Fourth Cumulant of Photo-assisted Shot Noise".

Chapter 1

Basics notions of statistical theory

The interpretation of different phenomena and experiments that occur in many fields and the study of electron transport are made possible through the analysis of statistical data. The present chapter is dedicated to the different techniques of analysis of random variables and consists of two sections: At first we will review the concepts of random variables, probability, probability distribution function, moments (mean and variance) and cumulants. An example of a Gaussian distribution will be studied and will allow us to clarify the relationship between cumulants and moments. Finally, in the second section we will discuss the notions of autocorrelation, correlation and spectral density, which are useful for noise analysis.

1.1 Random variables and probability distribution

1.1.1 Random variables

A random variable x is a function that map a random process to a number. For example, if a random process is to quantify if an electron crosses a barrier. Then, the random variable will be equal to one when an electron crosses the barrier (first outcome) and zero when it does not (second outcome). We notice from this example that the values of a random variable x ($\{x(t)\}$) depend on the outcomes of an experiment.

This means that the measurement of such variable from N identical systems will merely lead to different results $\{x_i(t)\}$; $i = 1, ..., N$ even if static conditions are applied (see figure 1.1). In such case, $\{x(t)\}$ corresponds to only one physical realization of what might have occurred in an experiment. Therefore, x can be characterized by the

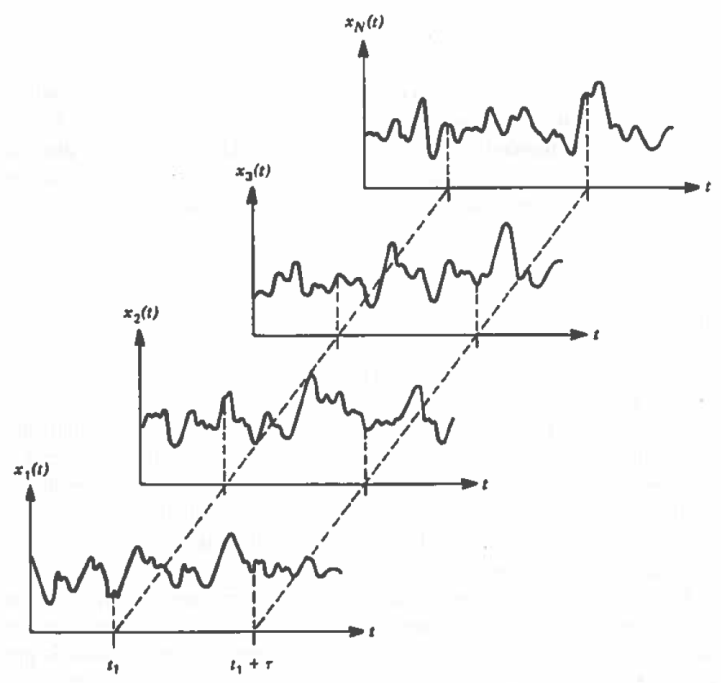

FIGURE *1.1:* Ensemble of time history recordings defining a random process [18].

following quantities: 1.) its mean value, 2.) the probability distribution functions, 3.) autocorrelation functions, 4.) power spectral density...

The mean value of x can be: on one hand computed for specific time t by averaging over all set possible data obtained from an ensemble of N identical systems given by

$$\mu_x(t) = \lim_{N \to +\infty} \frac{1}{N} \sum_{i=1}^{N} x_i(t) \tag{1.1}$$

On the other hand, computed over time from a single time history record

$$\bar{x}_i = \lim_{t_m \to +\infty} \frac{1}{t_m} \int_0^{t_m} x_i(t) dt \tag{1.2}$$

with t_m being the period at which data are taken. Experimentally, the latter is more often used and differs from the first case in the sense that there is no time dependence. These results can also be obtained knowing the probability of x [19].

1.1.2 Probability density function

The importance of probability density function has been highlighted and more proved in physics as well as in many other fields. As starting point let us recall what one means by probability before proceeding further.

Probability. The probability denotes the frequency at which an event occurs in a serial of tests. If a test is repeated N times and an event A occurs N_A times then the probability $P(A)$ for the A to occur is:

$$P(A) = \lim_{N \to +\infty} \frac{N_A}{N} \tag{1.3}$$

For a continuous process where the values of the event A are in between $-\infty$ and $+\infty$ as for a one dimensional random variable x the probability density function (PDF) given by:

$$p(x,t) = \frac{dP[x \leq x(t) \leq x + dx]}{dx} \tag{1.4}$$

is defined as the probability that the an outcome data of x at any instant of time; *i.e.* $x(t)$ has a value within x and $x + dx$. $p(x,t)$ is a real-valued positive function such that $\int_{-\infty}^{+\infty} dx\ p(x,t) = 1$.

For the special case of a stationary process, there is no time dependence ($p(x,t) \equiv p(x)$) and under the ergodic principle, one can demonstrate that $\mu_x = \bar{x}_i$ as set in previous equations.

1.1.3 Average and higher order moments

The average value or expectation of a continuous function g$[x]$ is given by:

$$\langle \mathrm{g}[x] \rangle = \int_{-\infty}^{+\infty} \mathrm{g}(x) p(x) dx \tag{1.5}$$

If $\mathrm{g}[x] = x^k$, then equation 1.5 can be rewritten as follows:

$$\mu_k = \langle x^k \rangle = \int_{-\infty}^{+\infty} x^k p(x) dx \qquad k = 1, 2, \ldots \tag{1.6}$$

This expression is nothing but than the moment of order k of the variable x whose *average* μ_1 is obtained when k equals to unity. The average of the square of the difference between the instantaneous and means value $\delta x = x - \mu_1$, calculated from the equation 1.6 gives

the *variance* of x; $\langle \delta x^2 \rangle = \mu_2 - \mu_1^2$. This quantity is of major importance because it measures the size of a typical fluctuation whose square root gives the *standard deviation* σ representing the width of the dispersion of the fluctuations.

1.1.4 Cumulants

Let the *characteristic function* of the moments μ_k be:

$$\begin{aligned} \phi_x(\lambda) &= \langle \exp(-i\lambda \mathbf{x}) \rangle \\ &= 1 + \sum_{k=1}^{\infty} \frac{(-i\lambda)^k \mu_k}{k!} \end{aligned} \tag{1.7}$$

$\phi_x(\lambda)$ is the Fourier transform of the probability distribution of the random variable x and λ a real parameter which is such that $\phi_x(\lambda = 0) = 1$. The nth order cumulants, C_n are defined as being the expansion coefficients of the logarithmic characteristic function of the moments:

$$\ln \phi_x(\lambda) = \sum_{n=1}^{\infty} C_n \frac{(-i\lambda)^n}{n!} \tag{1.8}$$

Let us first introduce the term on the right hand side (r.h.s) of the equation 1.7 in the one of the left hand side (l.h.s) equation 1.8. Later on, let us expand the resulting function, *i.e.* logarithmic function, and identify its nth order coefficients in $(-i\lambda)^n/n!$ with that on the r.h.s. This being done, we can show that there is a relationship between cumulants and moments where the first four terms are:

$$\begin{aligned} C_1 &= \mu_1 \\ C_2 &= \mu_2 - (\mu_1)^2 \\ C_3 &= \mu_3 - 3\mu_2\mu_1 + 2(\mu_1)^3 \\ C_4 &= \mu_4 - 4\mu_3\mu_1 - 3(\mu_2)^2 + 12\mu_2\mu_1^2 - 6\mu_1^4 \end{aligned} \tag{1.9}$$

In the particular case where $\mu_1 = 0$ (relevant for the experiment presented here) these cumulants can be redefined as: $C_2 = \mu_2$, $C_3 = \mu_3$, $C_4 = \mu_4 - 3\mu_2^2$.

The cumulants are very useful when we would like to separately analyze quantities that are mutually independent.

For example, if x and y are two random variables whose sum give rise to $S = x + y$. Then, the second moment of S ($\langle S^2 \rangle$) is equal to the sum of the second moment of x and

that of y; $\langle S^2\rangle = \langle x^2\rangle + \langle y^2\rangle$ since $\langle x\rangle = \langle y\rangle = 0$. In contrast to $\langle S^2\rangle$, the expression fourth moment of S gives in addition to the sum of the fourth moment of x and that of y, a product of second moment:

$$\langle S^4\rangle = \langle x^4\rangle + \langle y^4\rangle + 6\langle x^2\rangle\langle y^2\rangle \tag{1.10}$$

From this expression (1.10), we can conclude that $\forall n \geq 0\ \mu_n^S \neq \mu_n^x + \mu_n^y$. Furthermore, we can notice that it will be very difficult to extract $\langle x^4\rangle$ or $\langle y^4\rangle$ from the measurements of $\langle S^4\rangle$. Indeed, because x and y are very small therefore, we expect the product of their second moment to dominate the measured data of S. This difficulty can be overcome when investigating the cumulants since using the equations (1.7) and (1.8) one can show that $C_n^S = C_n^x + C_n^y$. This means that from the obtained data of C_n^S x can be analyzed knowing y, and vice versa. For example inverse Fourier transform of $\ln \phi_S(\lambda)$ the probability $P(S)$ which is equal to $P(S) = P(x) \times P(y)$.

1.1.5 Gaussian probability distribution

According to the central limit's theorem, the probability distribution of a large number of independent random variables $\{x_1, x_2, ...x_N\}$ with N $\to \infty$ is Gaussian:

$$p(x) = \frac{1}{\sigma\sqrt{2\pi}} \exp\left[-\frac{(x-\mu_1)^2}{2\sigma^2}\right] \tag{1.11}$$

This distribution has the following properties:

- It is perfectly symmetric around a mean value μ_1, so that all odd moments μ_{2k+1} are zero.
- It is totally defined by knowing its mean μ_1 and standard deviation σ^2, which represents the width of the distribution.

In such case, computing $\ln \phi_x(\lambda)$ leads to $i\lambda\mu - \frac{\lambda^2\sigma^2}{2!}$. Following equation (1.9), one can deduce that $C_1 = \mu_1$ and $C_2 = \sigma^2 = \mu_2 - \mu_1^2$ which are the only existing cumulants (*i.e.* $C_n = 0 \quad \forall n \geq 3$). So a necessary condition for a probability distribution to be Gaussian is that $\mu_4 = 3\ C_2^2$.

1.1.6 Autocorrelation functions

The autocorrelation function of x describes the general dependence between the measured outcome data at initial time t and that obtained at a future time $t+\tau$ [20]:

$$R_{xx}(\tau) = \langle x(t)x(t+\tau)\rangle = \lim_{t_m\to+\infty} \frac{1}{t_m}\int_0^{t_m} x(t)x(t+\tau)dt \tag{1.12}$$

1.2 Other statistical tools

We have shown in the first section that physical phenomena of single variable and their fluctuations can be rigorously described through the distribution probability. The joint properties of the two or many variables can however be determined when investigating correlation functions such as cross-correlation function and cross-spectral function.

1.2.1 Correlation

Suppose x and y be two variables simultaneously measured during a random process. Their joint probability distribution function defined as $P(x,y) = \int_{-\infty}^{x}\int_{-\infty}^{y} p(\zeta,\eta)d\zeta d\eta$ measures the probability to have at any time an outcome data $x(t)$ and $y(t)$ at most equal to x and y respectively with $p(\zeta,\eta)$ being the corresponding joint probability density function. The relationship between these different variables can be estimated when one valued the correlator of their fluctuations:

$$G_{xy} = \langle \delta x(t)\delta y(t+\tau)\rangle = R_{xy}(\tau) - \mu_x\mu_y \tag{1.13}$$

where the dependence between a value of x at time t and y at different time $t+\tau$ is described by the correlator $R_{xy}(\tau) = \langle x(t)y(t+\tau)\rangle$. This correlator called cross-correlation function is such that when $x(t) = y(t)$ we recover the auto-correlation function stated above (cf. equation 1.12).

For independent variables $G_{xy} = 0$, since $P(x,y) = P(x)P(y)$ implies that $R_{xy}(\tau) = \mu_x\mu_y$ so there is no relationship between the measured data.

1.2.2 Spectral density function

The spectral density function is the Fourier transform of the correlation function. In other words, if we consider previous examples, the spectral density between two recorded

data is expressed as:

$$S_{xy}(f) = \int_{-\infty}^{+\infty} d\tau R_{xy}(\tau) e^{-j2\pi f\tau} \tag{1.14}$$

It evaluates how random data are distributed with the frequency f. Similarly, one can define cross-spectral and power spectral density function when $x(t) \neq z(t)$ and $x(t) = z(t)$ respectively. The latter function $S_{xx}(f)$ as its name suggested is the power of the fluctuations at given frequency and is generally expressed as $S_{xx}(f) = \langle |x(f)|^2 \rangle = \langle x(f)x(-f) \rangle$.

Chapter 2

Fluctuations in tunnel junctions

In this chapter we present the theory of electronic fluctuations together with some experimental results for a tunnel junction. Following the scattering approach to the average electric current, conductance and characteristic noise properties such as spectral density, photo-assisted noise, noise susceptibility will be discussed. Prior to these discussions, we will attempt to give a brief definition of "noise" and its origins.

2.1 Noise: electronic current fluctuations

Because of its complexity, it is often difficult to give a universal definition of noise. Several suggestions are encountered in the literature. Some researchers like W. A. Rheinfelder [21] defined noise as unwanted signal with no physical interest. Others refer to it as a "perturbative" signal whose properties are only determined by statistics.

Nowadays, noise also called current fluctuations $\Delta I = I(t) - \langle I \rangle$ in electronics has become a sophisticated tool for investigating transport mechanism since its properties are statistically related to that of the entities which generate it [22]. In particular, quantum suppression and enhancement of noise in mesoscopic conductors have been predicted and evidenced to be strongly dependent to the behavior of electrons [23], which turn out to be controlled by the Coulomb interactions and/or Pauli exclusion principle.

For example, the correlated motion of electrons generally conducts shot noise suppression below its classical value $2eI\Delta f$ [23, 24]. This is due to the fact that Pauli principle tends to regulate the motion of the electrons and so reduces the fluctuations. Similar results have also been evidenced in several experiments [5, 25] or when dealing with half-integer charged carriers [26]. However, many interpretations have been with some

contradictions. This diversity in interpreting physical phenomena from their noise highlights the importance of the physics of electronic fluctuations. It is in that sense that Rolf Laudauer [5] said that: "noise is the signal", implying that its origins and characteristics need to be well understood.

2.1.1 Different types of noise

The characteristic features of noise depend on its multiple origins, which are either external or internal to the studied circuit. External sources of noise are electromagnetic perturbations caused by atmospheric disturbances, solar energy, cosmic rays, industries, etc. Internal sources are the components of a circuit itself, such as resistors, transistors, etc. When connected together, these components produce small current noise. At equilibrium ($V = 0$) and non-zero temperature, the small current noise is a direct consequence of thermal agitation of electrons, while when $V \neq 0$ it is due to charges quantization. A good review for noise origins is given by Ya.M. Blanter and M. Büttiker [11].

2.2 Electric properties of a tunnel junction

In this section, we will briefly present different types of junctions before addressing the properties of the tunnel junctions.

2.2.1 Definition

A junction is a thin insulating layer (I) sandwiched by two electrodes of same or different nature. When the properties of both electrodes are similar, the junction is said to be symmetric and the resulting properties are also symmetrical.

At the present, various types of junctions have been studied, and the most famous ones are the tunnel junction (N-I-N) separating two metallic electrodes (N), the Josephson junction (S-I-S) which involves two superconducting electrodes (S) and the asymmetric junction consisting of two dissimilar electrodes such as N-I-S.

All these conductors, in particular the tunnel junctions exhibit interesting properties. They have a relatively small thickness ($\approx$ nm to a few μm), a wide frequency band and a low transparency. The last property is such that the *Fano factor* quantifying the ratio between noise and the measured current [4] expressed as $F = \frac{\sum_n T_n(1-T_n)}{\sum_n T_n}$ [22] for a conductor containing N modes is approximately equal to unity; $F \approx 1$ with T_n being

transparency or transmission probability of the *nth* mode. In addition, due to the large frequency band B, the tunnel junctions produce a maximum of shot noise ($2eIB$). This is why they are qualified to be the simplest systems for noise measurement [17, 27–29].

2.2.2 Net average current in a tunnel junction

At equilibrium, when no bias voltage is applied to a system, the Fermi levels of both metallic reservoirs represented by μ_L and μ_R for the left (L) and right (R) reservoirs of the junction respectively coincide $\mu_L = \mu_R$ (see figure 2.1.*a*). At this point, the electric current through the junction is zero since there are as many electrons flowing forward as backward.

The application of a negative bias voltage V to the left reservoir will shift its Fermi level from that of the right reservoir inducing a potential difference eV. In this instance, the left metal is highly occupied while the right one is almost emptied (as shown figure 2.1.*b*) so that, the electrons can only tunnel from left to right. This will introduce a non zero average current.

The tunnel process is a concept introduced in quantum mechanics, for which a particle of low energy succeeds to pass through a potential barrier of higher energy. This phenomenon forbidden by classical mechanics (since the particle does not have enough energy to pass the barrier), is a consequence of the wave-particle duality [30].

According to this wave-particle theory, an elementary particle such as photon, electron, etc presents simultaneously wave and particle properties. It is the wave-like nature that allows a portion of the wave's amplitude of an electron incident to one side of the barrier to appear on the other side, while the remaining portion is reflected backward. In the first situation, the electron is said to be transmitted from left to right or from right to left with the transmission probabilities $T_{L\mapsto R}$ and $T_{R\mapsto L}$ respectively. In general, $T_{L\mapsto R} = T_{R\mapsto L} = T(E)$. These probabilities are thus proportional to the tunneling rate $\Gamma_{L\mapsto R}$ and $\Gamma_{R\mapsto L}$ respectively and from the Fermi golden rule, they are expressed in terms of the energy, the occupation number and the Fermi distribution function as:

$$\begin{aligned}\Gamma_{L\mapsto R} &\propto T(E)N_L(E)f_L(E)N_R(E)[1-f_R(E)]\\ \Gamma_{R\mapsto L} &\propto T(E)N_R(E)f_R(E)N_L(E)[1-f_L(E)]\end{aligned} \tag{2.1}$$

where $f_L(E) = f(E-eV)$ and $f_R = f(E)$ are the Fermi distribution functions of the left and right reservoirs respectively, with $f(E) = \frac{1}{e^{E/k_BT}+1}$. $N_L(E)$ and $N_R(E)$ are the

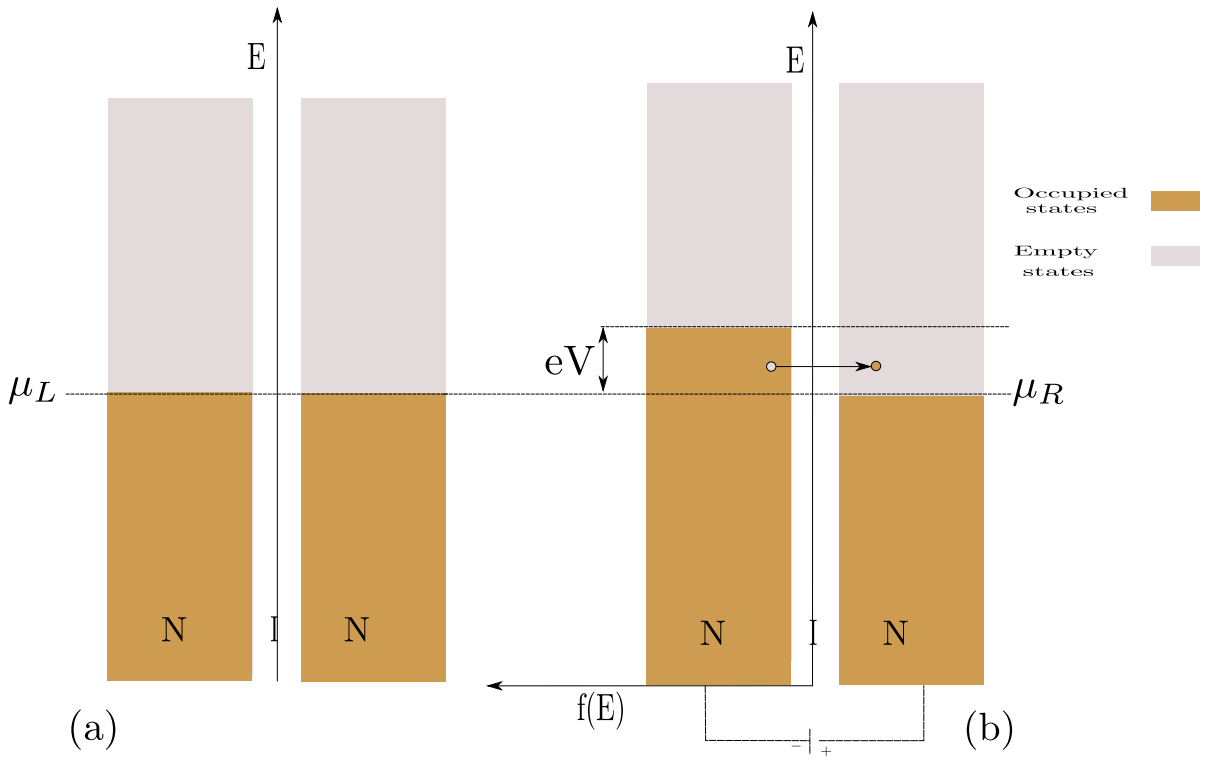

FIGURE 2.1: Energy diagram of a junction tunnel. a.) The equilibrium case when the voltage bias V = 0 V and T = 0. b.) For the non-equilibrium case $V \neq 0$, *i.e* the junction is polarized. In this case, there is a potential difference $-eV$ between left and right metals, with the left metal being at high potential.

number of states associated to the energies $E - eV$ and E respectively, with the factors $1 - f_{R(L)}(E)$ on hand, the transition into occupied states are not allowed; therefore they take into account the Pauli principle.

From these definitions, the net current across the junction, $\langle I \rangle$ can be computed for non-interacting electrons by averaging over energy the difference between the transmission rate of the left and right moving particle [31]; $\langle I \rangle = e \int_{-\infty}^{+\infty} \mathrm{d}E[\Gamma_{L\mapsto R} - \Gamma_{R\mapsto L}]$. If the number of states of both reservoirs are equal and slowly varying with energy so as to neglect their energy-dependence, *i.e.* $N_L(E) = N_R(E) = N_0 = cst$ and if the conductor of interest contains many parallel one-dimensional sub-bands (channels), each of which being characterized by constant transmission probability $T(E) = T$, then the net average current can be rewritten as:

$$\langle I \rangle = \frac{e^2 V}{2\pi\hbar} \sum_n T_n \tag{2.2}$$

since, $\int_{-\infty}^{+\infty} dE[\Gamma_L - \Gamma_R] = \int_{-\infty}^{+\infty} dE[f(E - eV) - f(E)] = eV$. Where T_n hereby describes the transmission probability for a particle traveling in the nth channel. e and $\hbar$ are the elementary charge of the electron and the Planck's constant h divided by 2π respectively. According to the Ohm's law, the conductance G is a current to voltage ratio (*i.e.* $G = I/V$) hereby equal to:

$$G = \frac{e^2}{2\pi\hbar} \sum_n T_n \tag{2.3}$$

This equation 2.3 is the multi-channel generalization of the Landauer formula [32].

2.2.3 Current noise spectral density of a tunnel junction

As described in the previous section, noise spectral density (NSD) called power spectral density is the Fourier transform of the average autocorrelation of the fluctuations. In time-domain, the autocorrelation for current fluctuations is given by:

$$A_i(\tau) = \langle \Delta I(t + \tau) \Delta I(\tau) \rangle_t \tag{2.4}$$

where $\langle \cdot \rangle_t$ means averaging over the absolute time t. f denotes the frequency at which the system is analyzed and τ is the time difference between current fluctuations. The

NSD in the frequency domain is therefore defined as [33]:

$$S_{ii}(f,V) = \int_{-\infty}^{+\infty} \mathrm{d}\tau e^{(i2\pi f\tau)} A_i(\tau) \tag{2.5}$$

which is a general formulation. For a non-stationary case where the current-current correlation function is periodic in the absolute time t, the calculus of the equation 2.5 can easily be done by first averaging over a period T the term on the r.h.s of equation 2.4 and then, transforming the resulting term $A_i(\tau)$ in the Fourier space to obtain $S_{ii}(f)$. The calculus becomes much more easier when dealing with a stationary case, since what matters is the time difference τ. In such case, the NSD for a phase-coherent mesoscopic conductor yields to:

$$S_{ii}(f,V) = F[S_0(eV/h+f) + S_0(eV/h-f)]/2 + (1-F)S_0(f) \tag{2.6}$$

where F is the fano factor defined above and $S_0(f)$ the spectral density at equilibrium (*i.e.* for $V = 0$) is given by $S_0(f) = 2hfG\coth\frac{hf}{2k_B\mathrm{T}}$.

Since for a tunnel junction $F \approx 1$, the last term on the r.h.s can then be neglected such that the NSD is reduced to $S_{ii}(f) = [S_0(eV/h+f) + S_0(eV/h-f)]/2$. This expression can be further simplified to:

1. $4\mathrm{k}_B TG$ when hf and $eV \ll \mathrm{k}_B T$.
2. $2eI$ when $eV \gg \mathrm{k}_B T$ and hf.
3. $2hfG$ when $hf \gg \mathrm{k}_B T$ and eV.

These noise limits correspond to the Johnson-Nyquist thermal noise [34], Poisson limit of shot noise and quantum zero-point noise respectively described above. In classical regime, the spectral density of noise for a tunnel junction is equal to that computed at $f = 0$ since there is no frequency dependence noise; $S_{ii}(f=0) = 2eI\coth\frac{eV}{2k_B\mathrm{T}}$.

2.2.4 Photo-assisted noise

To investigate the effect of additional a.c bias voltage on noise power spectral density, let us assume the electronic wave function for a quasi-particle of energy E under d.c bias V and in absence a.c bias to be given by:

$$\psi(r,t) = R(r)e^{-iEt/\hbar} \tag{2.7}$$

where $R(r)$ is a function which depends on the spatial coordinates. This function stands for the amplitude of wave function whereas $e^{-iEt/\hbar}$ is the phase factor. From the Hamiltonian's formalism, it is obvious that the presence of a.c bias voltage $V_{ac}\cos(2\pi f_0 t)$ will just shift the phase factor from its d.c value to $e^{-i(Et+\int_0^t eV_{ac}cos(2\pi f_0 t')dt')/\hbar}$. Consequently, when this quantity is expressed in terms of Bessel function $J_n(z)$, one can show that the new wave function is nothing but the superposition of wave functions whose energies are given by $E \pm nhf$; $\psi(r,t) = R(r)e^{-iEt/\hbar}\sum_{n=-\infty}^{+\infty} J_n(z)e^{(i2\pi nf)}$ where $z = \frac{eV}{hf}$. This means that several states are available for an electron tunneling [31, 35]. The spectral density of photo-assisted noise computed from the new wave function and in terms of the creation/annihilation operators [16] is therefore written as:

$$S_{ii}^{PA}(V,f) = \sum_{n=-\infty}^{+\infty} J_n^2(z)S_{ii}(V - nhf_0/e, f) \tag{2.8}$$

As we can noticed, the presence of a.c bias will not only change the section of energy that contributes to the transport from eV to $V - nhf_0$, but it will also make this section of energy oscillates. This will modify the spectral density $S_{ii}(V,f)$ at a given frequency. At low frequency (*i.e.* $f \to 0$) as in classical limit, $S_{ii}^{PA}(V,0)$ is equal to $\int_0^T S_{ii}(V + V_{ac}\cos 2\pi f_0 t, 0)\frac{dt}{T}$ because noise follows adiabatically the modulation of the energy levels of the electrons by the a.c bias excitation.

2.2.5 Noise susceptibility

Since the effect of a.c bias is to create new available states for an electron tunneling and to induce the oscillations of these states, in order to quantify how these states and the NSD measured at a given frequency oscillate with the number of harmonics excitation frequencies nhf_0, we will use:

$$X_n^+(f,f_0) = \langle i(f)i(nf_0 - f)\rangle - \langle i(f)\rangle\langle i(nf_0 - f)\rangle \tag{2.9}$$

with the first term on r.h.s being the correlator that described the dynamics of noise. For small and slow variations of the a.c bias voltage, the expression in the equation 2.9 can be approximated to $X_{\pm 1}(f)$ because the correlators $\langle i(f)i(nf_0 - f)\rangle$ for $|n| > 1$ have negligible contributions (c.f the formation of the side bands section(5.3)). This quantity $X_{\pm 1}(f)$ is interpreted as noise susceptibility [16] and measures the linear response of noise to a slow variation of oscillating excitation; $X_{\pm 1}(f) \propto \lim_{V_{ac}\to 0}\frac{dS_{ii}}{dV_{ac}^{f_0}}$ to be distinguished

from the adiabatic response proportional to $\frac{dS_{ii}}{dV}$.

Chapter 3

Relation between fourth cumulant of current and power fluctuations

The goal of this chapter is to understand the meaning of measured $G_2 = \langle P_1 P_2 \rangle - \langle P_1 \rangle \langle P_2 \rangle$ which defines the cross-correlation between power fluctuations of signals coming from two filters of non-overlapping bandwidth. Furthermore, one would like to know how it can be related to the fourth cumulant $C_4 = \langle i(t)^4 \rangle - \langle i(t)^2 \rangle^2$ of current noise, *i.e.* correlation of four currents at different frequencies (cf. appendix A). We begin by investigating the autocorrelation of power fluctuations before studying G_2.

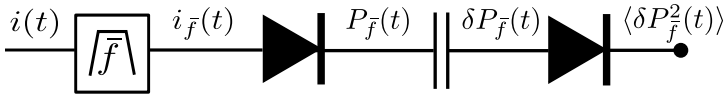

FIGURE 3.1: Simplified diagram of the autocorrelation of power fluctuations associated to a signal filtered at central frequency $\bar{f}$ of a bandpass filter; $i_{\bar{f}}(t)$.

3.1 Autocorrelation

Let $i(t)$ be the current at the input of a bandpass filter centered at frequency $\bar{f}$ as depicted in figure 3.1. Before entering the filter, the current can be expressed in the Fourier space as the integral of a frequency response function $i(f)$ over all positive and negative frequencies. Since $i(t)$ is a real quantity, its Fourier amplitude obeys $i(-f) = i^*(f)$. The

Fourier integral is then:

$$i(t) = \int_0^\infty \mathrm{d}f[e^{i2\pi ft}i(f) + e^{-i2\pi ft}i(-f)] \tag{3.1}$$

thus, $\langle i(t)\rangle = 0$.

At the filter, some of the frequencies of the signal are filtered out and the remaining ones are within a band frequency from $\bar{f} - \Delta f/2$ to $\bar{f} + \Delta f/2$. The random signal $i_{\bar{f}}(t)$ at the output of the filter will thus be given by:

$$i_{\bar{f}}(t) = \int_{-\Delta f/2}^{\Delta f/2} \mathrm{d}\epsilon[e^{i2\pi(\bar{f}+\epsilon)t}i(\bar{f}+\epsilon) + e^{-i2\pi(\bar{f}+\epsilon)t}i(-\bar{f}-\epsilon)] \tag{3.2}$$

where ϵ is any frequency within the bandpass of the filter. When this signal reaches the input of the diode, it will be squared and so its corresponding instantaneous power $P_{\bar{f}}(t)$ will introduce terms of high and low frequencies.

Since we are interested in measuring the correlation between power fluctuation at low frequencies, all quantities that involve frequencies such as $i(\pm\bar{f} \pm \epsilon)$ and $i(\pm\bar{f} \pm \epsilon')$ will therefore be omitted.

Thus, $P_{\bar{f}}(t)$ is expressed as:

$$P_{\bar{f}}(t) = 2 \iint \mathrm{d}\epsilon\mathrm{d}\epsilon'[e^{i2\pi(\epsilon-\epsilon')t}i(\bar{f}+\epsilon)i(-\bar{f}-\epsilon')] \tag{3.3}$$

This quantity proportional to the output voltage at the diode, when time-averaged gives the d.c part of $P_{\bar{f}}(t)$ (that is $\epsilon = \epsilon'$):

$$\langle P_{\bar{f}}\rangle = 2 \int \mathrm{d}\epsilon\ i(\bar{f}+\epsilon)i(-\bar{f}-\epsilon) \simeq 2\Delta f\langle|i(\bar{f})|^2\rangle \tag{3.4}$$

which nothing but $\langle P_{\bar{f}}\rangle = 2\Delta f S(\bar{f})$ where $S(\bar{f})$ is the spectral density of current noise at $\bar{f}$; $S(\bar{f}) = \langle i(\bar{f})i(-\bar{f})\rangle$. The presence of a capacitor allows only power fluctuations $\delta P_{\bar{f}}(t)$ to pass through it. The latter, from the equation 3.3 is such that $\epsilon \neq \epsilon'$. By averaging out the square of the latter power fluctuations at the output second diode, one can obtain the autocorrelation function

$$\langle \delta P_{\bar{f}}^2(t)\rangle = 4 \int \mathrm{d}\epsilon\mathrm{d}\epsilon'\mathrm{d}\xi\mathrm{d}\xi'\langle i(\bar{f}+\epsilon)i(-\bar{f}-\epsilon')i(\bar{f}+\xi)i(-\bar{f}-\xi')\rangle\delta(\epsilon-\epsilon'+\xi-\xi') \tag{3.5}$$

for which the calculation includes several non-vanishing terms:

1. The d.c power $\langle P_{\bar{f}}\rangle^2$ obtained when $\epsilon = \xi'$ and $\xi = \epsilon'$ since $\epsilon = \epsilon'$ and $\xi = \xi'$ are forbidden by the capacitor.

2. The fourth cumulant $C_4(\bar{f}, \bar{f}+\Delta, 0) \propto \langle i(\bar{f})i(-\bar{f})i(\bar{f}+\Delta)i(-\bar{f}-\Delta)\rangle$ (see appendix A.6) obtained when the frequencies are different, that is:

   (a) $\epsilon - \epsilon' = \Delta$ and $\xi - \xi' = -\Delta$

   (b) $\epsilon + \xi' = \Delta$ and $-\epsilon' - \xi = -\Delta$

   (c) $\pm(\epsilon - \xi') = \pm\Delta$ and $\pm(\xi - \epsilon') = \mp\Delta$ where Δ is a small frequency that passes the capacitor.

For a **Gaussian fluctuation** the fourth cumulant vanishes and therefore the only term remaining in equation 3.5 is the squared d.c power; $\langle \delta P^2_{\bar{f}}(t)\rangle = \langle P_{\bar{f}}\rangle^2$. Whereas, for a **non-Gaussian fluctuation** both terms of the C_4 and $\langle P_{\bar{f}}\rangle^2$ will survive.

3.2 Cross-correlation

Considering the measurement diagram of the cross-correlation depicted in figure 3.2 there are two non-overlapping filters centered at $\bar{f}_1$ and $\bar{f}_2$. The equation 3.5 in this case can be rewritten as:

$$\langle \delta P_1(t)\delta P_2(t)\rangle \simeq \int \mathrm{d}\epsilon\mathrm{d}\epsilon'\mathrm{d}\xi\mathrm{d}\xi' \langle i(\bar{f}_1+\epsilon)i(-\bar{f}_1-\epsilon')i(\bar{f}_2+\xi)i(-\bar{f}_2-\xi')\rangle \delta(\epsilon-\epsilon'+\xi-\xi') \tag{3.6}$$

where $\{\epsilon, \epsilon'\}$ and $\{\xi, \xi'\}$ are within different filters, *i.e.* $\bar{f}_1 + \epsilon \neq \bar{f}_2 + \xi$. The calculus of the above equation 3.6 does not include any squared d.c power $\langle P_{\bar{f}}\rangle^2$ since $\epsilon - \epsilon' \neq 0$ and $\xi - \xi' \neq 0$ (because of the capacitors). The only term that is involved is proportional to $\langle i(\bar{f}_1+\epsilon)i(-\bar{f}_1+\epsilon+\Delta)i(\bar{f}_2+\xi)i(-\bar{f}_2-\Delta+\xi)\rangle$ obtained when $\epsilon - \epsilon' = \Delta$ and $\xi - \xi' = -\Delta$ or ... This term is a fourth cumulant $C_4(\bar{f}_1, \bar{f}_2, 0)$ since all frequencies are different.

For Gaussian noise, $\langle \delta P_1 \delta P_2\rangle = 0$.

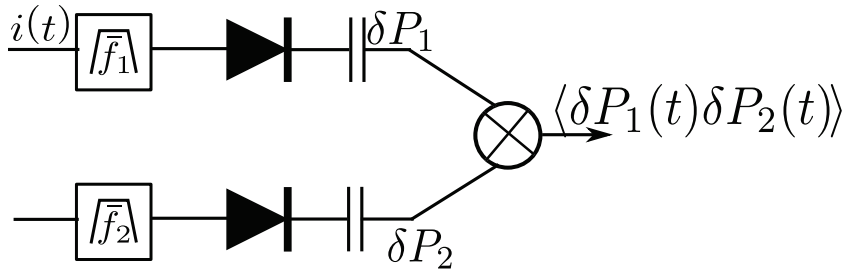

FIGURE 3.2: Schematic diagram of a basic circuit for the measurement of cross-correlation between power fluctuations of time-dependent electrical current emanating from two independent filters of central frequencies f_1 and f_2. The current $i(t)$ at input of the filters are coming from the same source that here the tunnel junction.

3.3 Summary

To summarize, we have shown that both auto and cross-correlation of power fluctuations of noise are related to the fourth cumulant C_4 of current and their expressions are given by $\langle \delta P_{\bar{f}}(t)^2 \rangle = \langle P_{\bar{f}} \rangle^2 + C_4(\bar{f}, \bar{f} + \Delta, 0)$ and $\langle \delta P_{\bar{f}_1}(t) \delta P_{\bar{f}_2}(t) \rangle = C_4(\bar{f}_1, \bar{f}_2, 0)$ respectively.

Chapter 4

Preliminaries and experiment

In the first chapter, we will present in the first section the preliminary steps of the experiment and in the second one, we will describe the core of the experiment which consists in measuring the correlation between power fluctuations of noise G_2 and the fourth cumulant C_4 of current fluctuations from an histogram method.

4.1 Preliminaries

The first steps toward the measurement of $G_2 = \langle P_1 P_2 \rangle - \langle P_1 \rangle \langle P_2 \rangle$ in a tunnel junction consisted in characterizing the sample, choosing an adequate circuit for the experiment and then optimizing its overall gain of the detection as well as the acquisition card. These steps are detailed in the following subsections.

In subsection 4.1.1, we will briefly introduce the sample and characteristics. Then, in subsection 4.1.2 and subsection 4.1.3 we will present a simple noise measurement and photo-assisted noise measurement respectively before optimizing the signal to noise ratio (in subsection B.2).

4.1.1 Sample characterization

Our sample was an Al/Al oxide/Al tunnel junction similar to the one used for noise thermometry [36]. We start its characterization by first measuring its resistance R_S at room and low temperature this in order to verify if it is properly functioning.

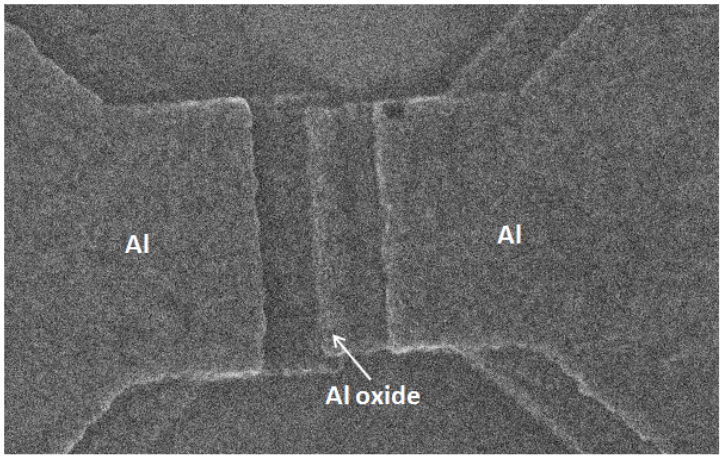

FIGURE 4.1: Top view picture of a tunnel junction.

Measurement of resistance

One way to measure the resistance of a sample is to place it in a voltage divider with a large load resistor R_L ($R_L \gg R_S$) in order to convert the bias voltage into current. This current will pass through the sample and the voltage drop V_S it generates across the resistance R_S will be measured by a voltmeter mounted in parallel (as shown in the figure 4.2). In this study, we used a lock-in amplifier as both source and detector (voltmeter) of signal. The load resistor and bias voltage were fixed at R_L = 1 MΩ and 1 V respectively. As a result, the bias current was approximately equal to $I_{bias} = \frac{V_{bias}}{R_S+1\ M\Omega} \approx$ 1 μA. Thus, when the sensitivity of the voltmeter was adjusted to μV, the voltage drop V_S read from it directly gave the resistance R_S.

This procedure was used for both measurement at 300 K and 4.2 K. The resulting data shown in the table 4.1 presents reasonable values of R_S.

Therefore, we investigated the characteristics of noise spectral density (NSD) as function of the applied voltage S_{exp} vs V.

	Temperature K	Resistance R_S Ω
Room	300	26.36
Cryostat ^{4}He	4.2	22.8

TABLEAU 4.1: Variation of the resistance of the sample as function of temperature.

.

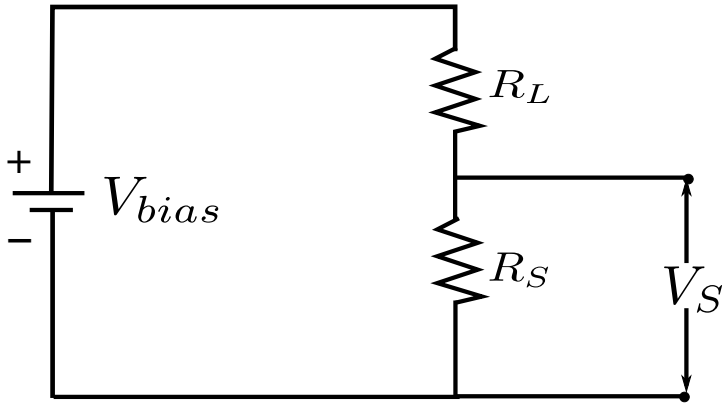

FIGURE 4.2: Voltage divider circuit biased at a voltage V_{bias} and $V_S \simeq R_S I_{bias}$.

4.1.2 Characteristic of noise spectral density S_{exp} vs V

To determine the characteristics of the NSD for our sample, we measured its noise for various d.c bias voltages.

Noise measurement

Measurement device

A simple circuit for noise measurement depicted on figure 4.3 contains:

1. The sample (a tunnel junction) of the resistance R_S.
2. A voltage source with a resistor 100 kΩ to bias the sample in d.c current.
3. A bias Tee to separate the d.c and Radio frequency (RF) current and thus to prevent the d.c bias current supplied by the current source from arriving at the amplifier.
4. An amplifier to amplify the noise generated by the sample which is of very low amplitude.
5. A bandpass filter to select the frequency f and the bandwidth Δf at which noise was measured.
6. A detector: a diode, to transform the input noise power associated to squared amplitude of the filtered noise into an output voltage; $V_{diode} = kP_{in}$ with k the conversion factor.

7. A voltmeter to read out the output d.c voltage at diode.

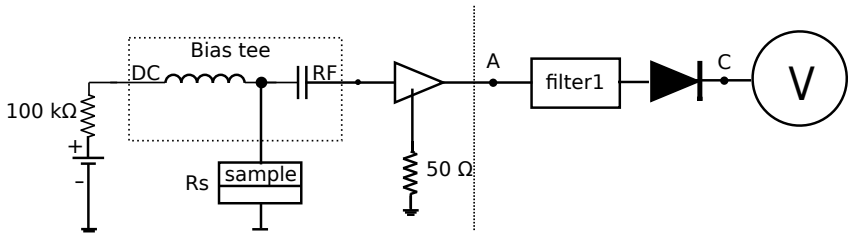

FIGURE 4.3: Simplest device for noise measurement.

Principle of the measurement

A d.c bias voltage V_{dc} varying from -10 to 10 V was supplied using a voltage source connected to a load resistor of resistance R_L hereby fixed to 100 kΩ this to impose a average current between -100 to 100 μA. This current passed through the d.c port of the bias Tee (containing the inductance) before reaching the resistance R_S of the sample which was then biased. The latter being polarized, it emitted an a.c current $i(t)$ within a large band frequency that traveled along the a.c port of the bias Tee (containing the capacitor) to arrive at the amplifier whose input resistance R_0 = 50 Ω. Given that the amplifier was not ideal, it superposed its intrinsic current noise $i_0(t)$ to $i(t)$ and amplified the overall current. The output signal was given by $\delta V_A = AR_T(i(t) + i_a(t))$, with A the gain of amplifier and $R_T = \frac{R_S R_0}{R_S + R_0}$. Thus, the voltage fluctuations are expressed as:

$$\langle \delta V_A^2 \rangle = 2\Delta f S_{VV} \tag{4.1}$$

with $S_{VV} = A\ R_T^2(S_{ii} + S_{i_0 i_0})$ being the spectral density for voltage fluctuations hereby related to S_{ii} and $S_{i_0 i_0}$ which are the spectral density of the fluctuating current from the sample and the amplifier respectively. Δf is the bandwidth of the amplifier. The factor 2 takes into account the fact that both negative and positive frequencies analyzed [1].

The d.c voltage at point C, V_C measured by the voltmeter was such that $V_C \propto \alpha S_{VV}$. α is the overall gain of the detection (Hz V^{-1}) which takes into account the conversion factor k of power to voltage, the detection bandwidth Δf_D of the filters, of the diode and parasitic band-frequency and R_0 = 50 Ω the resistance of the detector; $\alpha = 2kR_0\Delta f_D$.

Since we are concerned in measuring the NSD of the sample $S_{exp}(V)$, to properly analyze the data, the contribution of the NSD of the amplifier was removed from the

[1] because S_{ii} hereby represents half of the value defined in subsection 2.2.3; $S_{ii} = eI \cos \frac{eV}{k_B T}$

measured one. It results therefore from the equation 4.1 that $S_{exp} = AR_T^2 S_{ii}$. For $S_{ii} = eI$, S_{exp} is maximal for $R_S \to R_0 = 50\ \Omega$ (as shown in figure 4.4). This why we chose R_S of the order of 50 Ω.

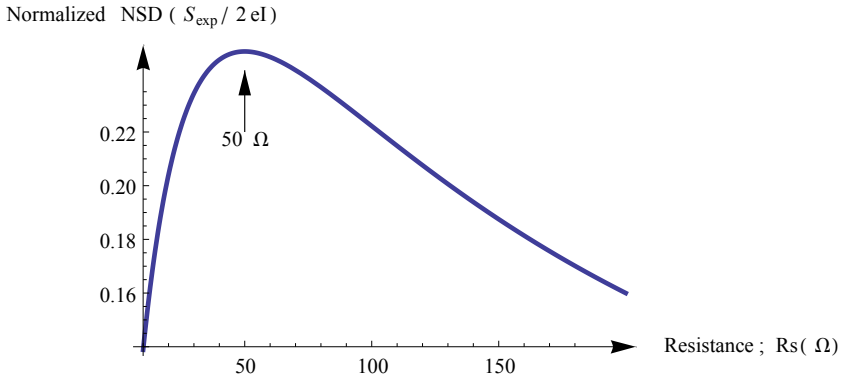

FIGURE 4.4: The optimal condition for measuring maximum noise: curve of the normalized NSD $\frac{S_{exp}}{AeI} = R_T^2$ with $R_T = \frac{R_S R_0}{R_S + R_0}$.

Noise characteristics $S_{exp}(V)$

The figure 4.5 represents the theoretical curve of the equivalent Johnson-Nyquist noise temperature for a tunnel junction obtained by normalizing the spectral density S_{VV} in $V^2\ Hz^{-1}$ with $2Gk_BAR_T^2$; $T^* = S_{VV}/(2Gk_BAR_T^2)$ where $G = 1/R_S$ is the conductance of the sample. As we can notice from this figure, the characteristics T^* vs voltage directly leads to the electronic temperature T_e and the noise temperature of the amplifier T_a.

The figure 4.6 illustrates the variation of the experimental data of V_C collected at the output of the diode for a signal emanating from a filter VBF–4440$^+$ + VLF-5500$^+$ (3.2–5.2 GHz) as function of the bias voltage V_{dc}. For clarity, we transform the real data in volts units into K units by normalizing them with α hereby expressed in $V\ K^{-1}$. Experimentally, α, T_e and T_a are the best parameters for the function $T^* = \alpha[T_e\ x \coth x + T_a]$ that fit the curve of the real data of V_C vs V_{dc} and their values are equal to 0.246×10^{-3} V K^{-1}, 2.82 K and 10.16 K. We notice that $T_e = 2.82$ K is approximately equal to the temperature of the cryostat fixed to 3 K. To obtain the characteristics of the spectral density for the sample S_{exp} vs V_{dc} we need to remove the contribution T_a from the data in figure 4.6.

At first sight, our sample is seems to perfectly function because theory and experiment are in good agreement.

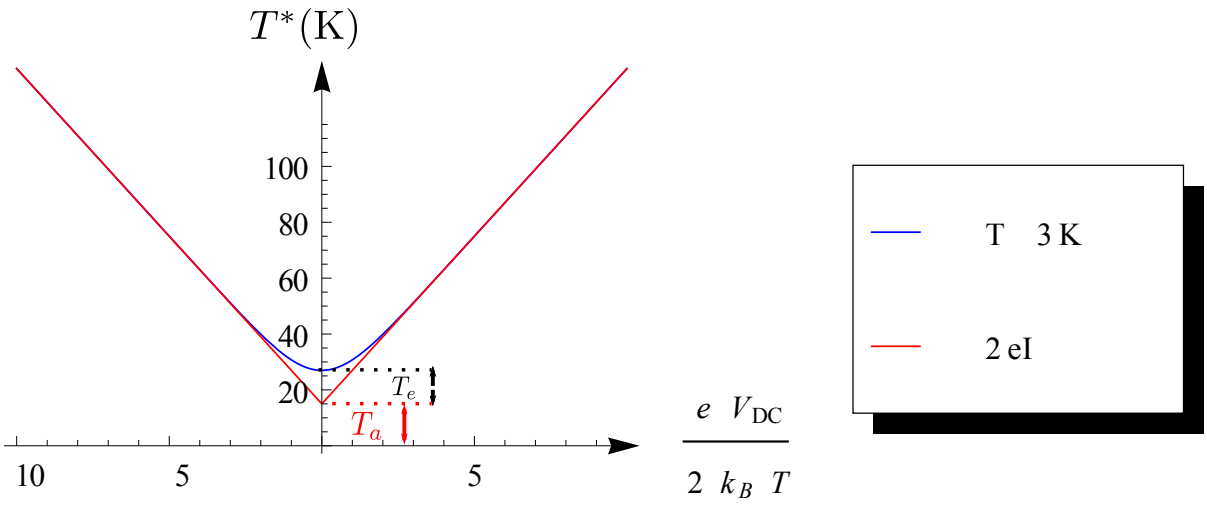

FIGURE *4.5:* Theoretical diagram of the characteristics of noise equivalent temperature for a tunnel junction in K; $T^* = \frac{S_{VV}}{2Gk_BAR_T^2} = [T_e\ x\coth x + T_a]$ with the overall gain of the detection being equal to $\alpha = 1$, $T_a = S_{i_0i_0}/4G_0k_B$ and T_e and $x = \frac{eV}{2k_BT_e}$ being the noise equivalent temperature of the amplifier and that of electron respectively. Where $G_0 = 1/R_0$ is conductance of the amplifier. Red line represents Shot noise spectral and blue line is NSD at 3 K.

4.1.3 Photo-assisted noise (PAN); S_{exp} vs V_{dc}

Measurement device

Photo-assisted noise can be investigated using the circuit in figure 4.7. This circuit contains in additional components besides those presented in the previous subsections:

1. A r.f source which supplied an a.c voltage to bias the sample.

2. A coupler which is a symmetric device hereby designed in manner that: 97% of the inputed signal (P_{in}) from the port-1 and 3% of the signal P_{ac} coming from the port-3 (supplied by r.f source), travelling forward in the main transimission go to the output port-4 while the remaining portions the former signals (3% of P_{in} and 97% of the P_{ac}) go to the 50 Ω terminal internal of the coupler (*i.e.* port-2). Since the coupler is symmetric, an inverse situation will occur for the signals travelling backward in the main transmission (*i.e.* from port-4 to port-3). In such case, 3% of P_{in} and 97% of P_{ac} coming from the port-4 will go to the port-1 and port-3 respectively.

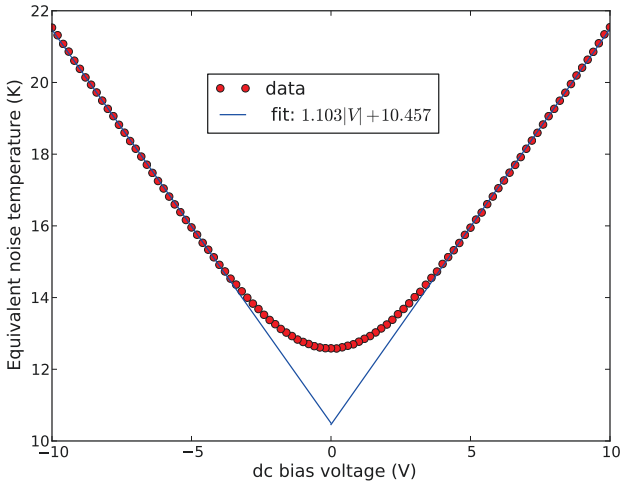

FIGURE 4.6: The characteristic curve of the NSD (V_C) vs V_{dc} in K unit with the offset due T_a = 10.16 K, $\alpha = 0.246 \times 10^{-3}$ V K^{-1} and T_e = 2.82 K. Red points are experimental data and in blue line is a fit function of the corresponding shot noise.

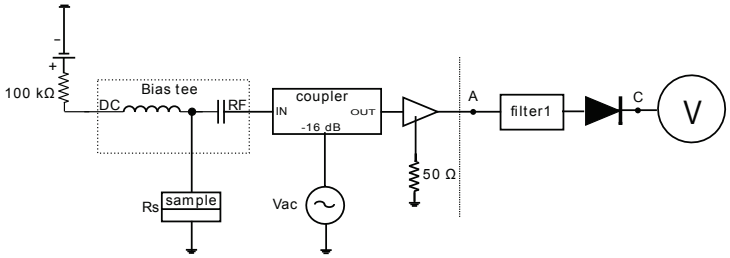

FIGURE 4.7: Simplest device for the measurement of photo-assisted noise.

Principle of the measurement. Consider the measurement circuit in figure 4.7. An r.f source connected through a coupler to the sample supplies an a.c voltage V_{ac} at frequency f_0. This voltage is at first attenuated at input port of the coupler before it is superposed to the d.c bias. Since, the effects of the a.c bias voltage is to modulate adiabatically the energy levels of the electrons (cf. chapter 2). Therefore, for every d.c bias voltage (from -10 to 10 V) we expect, the current emitted by the sample for a given a.c excitation to oscillate at f_0 by quantity GV_{ac} around its d.c values. In such case, the averaged voltage fluctuations measured at point at point C (PAN) are given by:

$$V_C \propto \bar{S}(V_{dc}, V_{ac}) = \int_{-\pi}^{\pi} S_{ii}(V_{dc} + V_{ac}\cos\omega_0 t)\frac{d(\omega_0 t)}{2\pi} \tag{4.2}$$

where $\omega_0 = 2\pi f_0$.

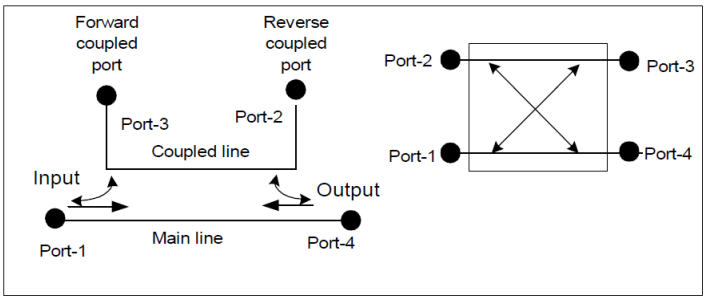

FIGURE 4.8: Schematic diagram of a coupler.

As we can notice from the PAN is nothing but the modulation of the conventional noise. So it is useful when calibrating the V_{ac} at sample. Theoretically we get figure 4.9 and experimentally we have the figure 4.10. Both figures, show a remarkable change of the amplitude of the PAN at low d.c bias ($-2 \geq V_{dc} \leq 2$), in contrast to high d.c bias ($V_{dc} \geq 3$ V or ≤ -3 V) where there is no change at all.

For $V_{ac} \ll 1$, $S_{ii}(V_{dc} + V_{ac}\cos\omega_0 t)$ can be expanded in power of $V_{ac}\cos\omega_0 t$ so that the value of V_C computed from equation 4.2 will yield to $\frac{V_{ac}^2}{4}\frac{d^2 S_{ii}}{dV^2}|_{V_{dc}}$. The latter quantity as we can noticed from the figure 4.11 illustrating the second derivative of S_{ii} will be maximal at low d.c bias voltage (*i.e.* when $V_{dc} \to 0$) and minimal when the bias is maximal. One may conclude therefore that the variation of the PAN at low bias is mainly due to $\frac{d^2 S_{ii}}{dV^2}$.

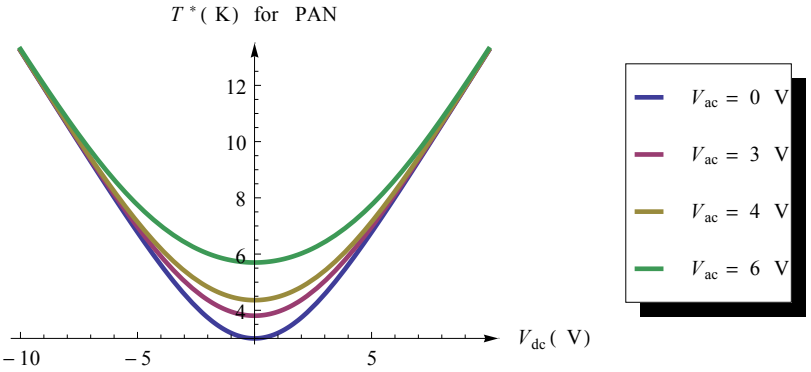

FIGURE 4.9: Theoretical curve of the PAN vs V_{dc} illustrating the function in equation 4.2 for various amplitudes of V_{ac}.

Based on the observations, the data obtained for both noise and photo-assisted noise measurements agree well with theory. To further characterize noise and design the optimal circuit for the measurement G_2, we conducted many tests in different circuits for

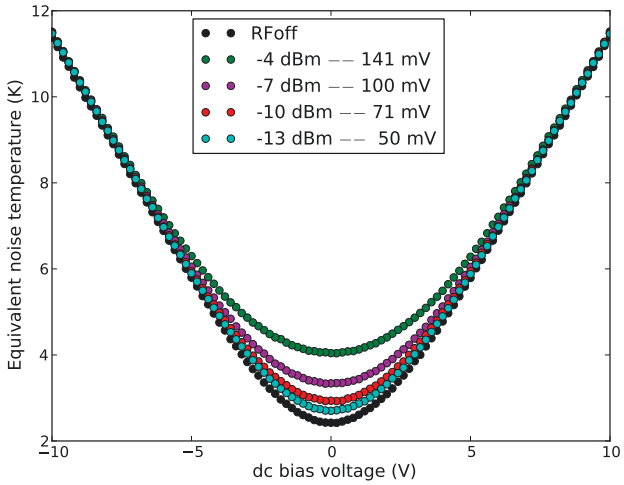

FIGURE 4.10: Experimental curve of the PAN vs V_{dc} for various amplitude of V_{ac} at f_0 = 11.6 GHz when the offset T_a of the amplifier is removed. The data that are drawn here were filtered around 4.5 GHz using a bandpass filter: VBF–4440$^+$ + VLF-5500$^+$. The characteristics of this bandpass filter can be found in table B.2 in appendix B.2.1.

which T_e, T_a, α and the signal to noise ratio (SNR) have been explored. The resulting data and detailed experiments can be found in the table **??** in the appendix B).

4.2 Experiment

4.2.1 Experiment set-up

The measurement concept of G_2 is illustrated in figure 4.12 which is a simplified diagram of the circuit 3 pictured in the figure B.3. The sample A within a cryostat at 3 K (region below the delimiter line) was current biased by a d.c voltage source connected to 100 kΩ resistor and a.c voltage biased below 4 GHz and above 8 GHz using two microwave sources (in a region at 300 K above the delimiter). The a.c current emitted by the former (from d.c – 18 GHz) was first filtered and amplified by a cryogenic amplifier of bandwidth frequency 4–8 GHz connected to a triplexer. The output signal was then symmetrically split before passing through two filters. The first filter, LF was centered at f_1 = 4.5 GHz and has a bandwidth frequency Δf_1 = 0.72 GHz while second one, HF had a central frequency f_2 = 7.15 GHz and bandwidth Δf_2 = 0.60 GHz. At each branch of the circuit, a DTM180AA diode integrated over time $t_m = 1/(100\ \text{MHz})$ the power

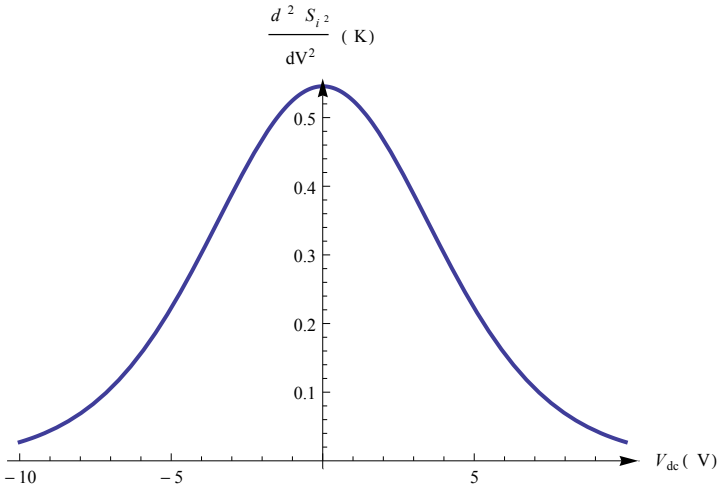

FIGURE 4.11: Second derivative of the NSD of tunnel junction vs V_{dc} with S_{i^2} equivalent to S_{ii}.

associated to the square of the filtered current coming from the filters. The resulting the power at the point B_k proportional to the voltage $v_k(t) = \langle v_k(t)\rangle + \delta v_k(t)$ passed across capacitors which blocked the $\langle P_k\rangle \propto \langle v_k(t)\rangle$ where $k = 1, 2$. $\delta P_1(t) = P_1(t) - \langle P_1\rangle$ and $\delta P_2(t) = P_2(t) - \langle P_2\rangle$ at the points C_1 and C_2 respectively were then digitized by a 2-channels, 14 bit, 400 MS/s acquisition card before the auto- and cross-correlation ($\langle \delta P_k^2\rangle$ and $G_2 = \langle \delta P_1 \delta P_2\rangle$ respectively) were computed. Prior to that, the effective power at the sample was calibrated.

4.2.2 Calibration of the effective power at the sample; P_S

Following the experiment setup of figure 4.12, an excitation power deliberated by a.c sources passed through a resistor, attenuators, bias Tee and filters before reaching the sample, therefore, it went under a series of attenuations. In addition, there was a mismatch in impedance between the resistance of the sample and that of the commercial detectors (50 Ω) so we knew for sure that the amplitude of a.c power was reduced when it reached the sample. So, we had to calibrate the amplitudes of the excitation power in order to have a control on the effective power arriving to the sample P_S, thus to avoid damages.

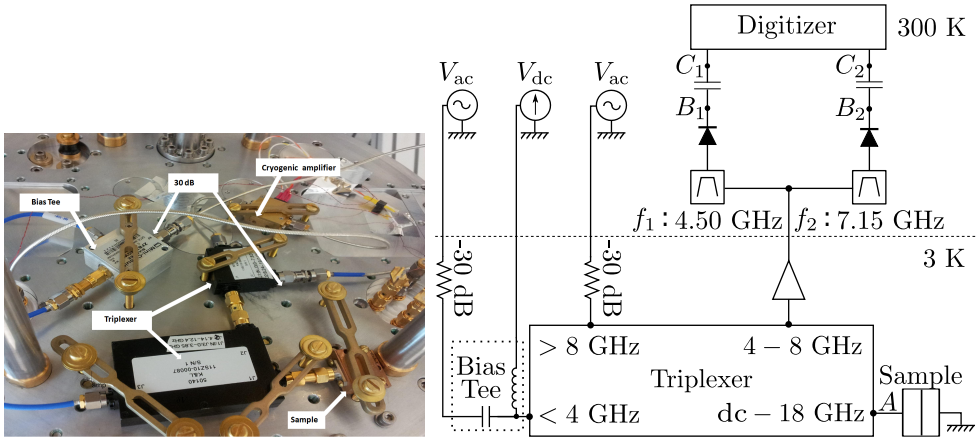

(a) Crystat (b) Experimental setup.

FIGURE 4.12: Schematic representation of the experimental setup. a.) real picture of the components inside of the cryostat. b.) Schematic diagram of the measurement circuit.

4.2.3 Calibration of the effective power at sample P_S at very low a.c bias

To calibrate the effective power at the sample, we first measured the PAN at low frequency. The bias voltage V_{dc} was fixed to 0 V and the a.c frequency was set to 2007 Hz while sweeping the amplitude of V_{ac} from 4 mV to 5 V using a lock-in amplifier connected to a 100 kΩ resistor as shown in figure 4.13. This frequency 2007 Hz was very low that the reflections due to the presence of long cables or mismatching impedances between the sample and components directly connected to it were negligible. Consequently, it was as if the current associated to V_{ac} supplied by the a.c source only passed through an external resistance of 100 kΩ before arriving at the sample R_S (in series). In this situation, the effective power at sample P_S was theoretically expressed as: $P_S = \frac{2V_{ac}^2 R_S}{(R_S+100\ \text{k}\Omega)^2}$. The factor 2 took into account the root means squared value of peak–peak amplitude V_{ac}. The data of the PAN measured at point B_k vs V_{ac} for the two filters are represented in figure 4.14. When these data are plotted in function of P_S we got the curves in figure 4.15 where P_{SLF} and P_{SHF} are the fit functions of the curves P_S vs noise temperature for a signal from the LF (B_1) and HF (B_2) respectively. These functions are linearly varying with noise temperature so given any value of noise, one can calculate the effective power at sample using the formers. At this point, the P_S is said to be calibrated at 2007 Hz. Another way of calibrating the effective power at given V_{ac} and excitation frequency is

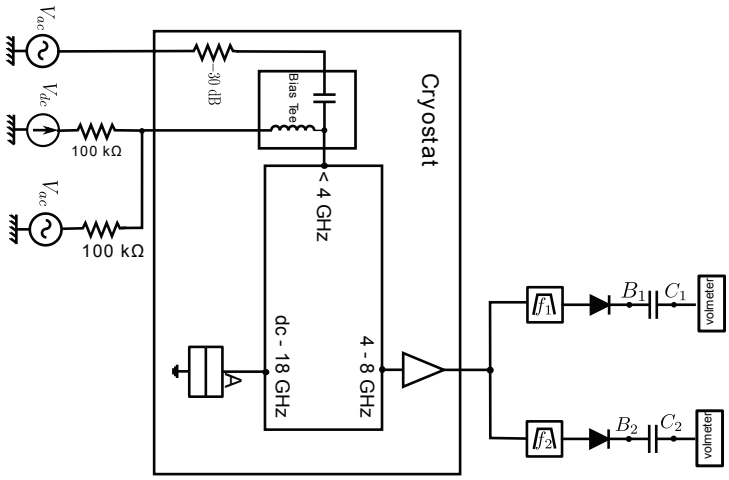

FIGURE 4.13: Experimental setup for the calibration of the effective power at sample. At $V_{dc} = 0$ V, $I_{ac} = \frac{V_{ac}}{(R_S + 100\ \text{k}\Omega)}$ and $P_S = R_S I_{ac}^2$ with V_{ac} being in peak–peak amplitude and has to be expressed in rms.

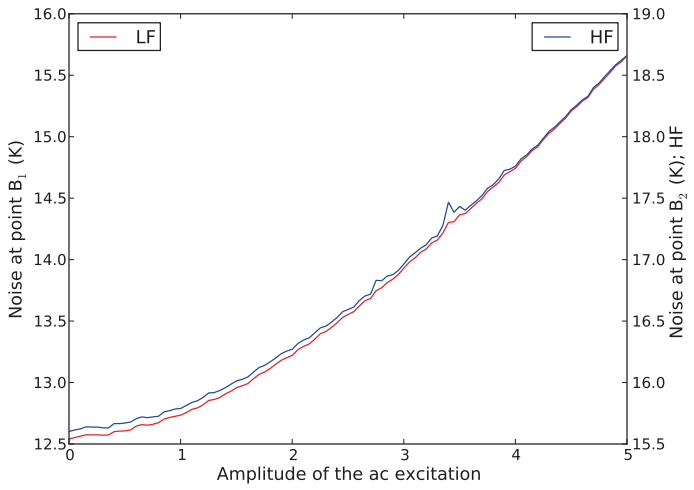

FIGURE 4.14: Calibration of the effective power at low a.c excitation (*i.e.* 4 mV$\leq V_{ac} \leq$ 5V and $f_0 = 2007$ Hz): Curve representing the variation noise equivalent temperature as function of the a.c voltage when $V_{dc} = 0$ V. The obtained data of noise in volts unit were normalized by the α which is equal to 0.246×10^{-3} V K^{-1} when they are from the low filter, LF (red line) and 0.233×10^{-3} V K^{-1} for the high pass filter, HF (blue line).

to measure PAN as a function of V_{dc} for various powers P_{ac}[2] and frequencies f_0 of the excitations. The recorded data in figure 4.16 can be fitted with equation 4.2 since in this dissertation, the excitation energy is always negligible compared to the thermal energy of electron ($hf_0 \ll k_B T$) so the PAN can be well approximated by the equation 4.2 which behaves as if there is no frequency dependence.

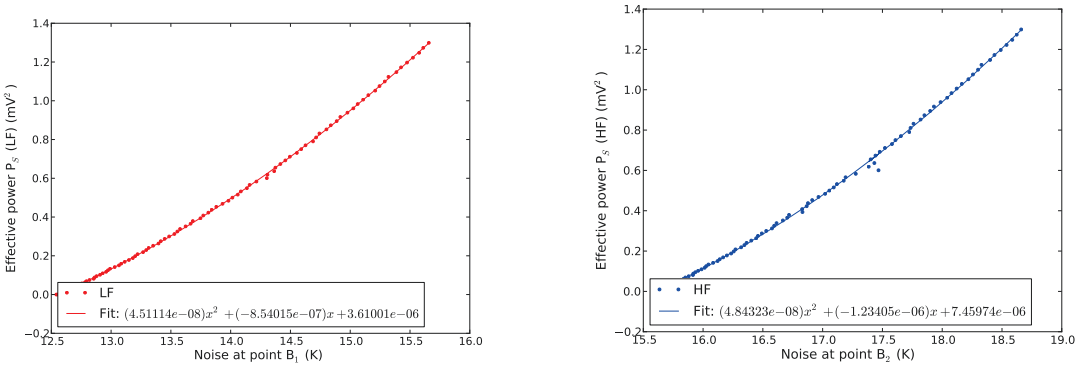

(a) LF (b) HF

FIGURE *4.15:* Variation of the effective power at the sample P_S as function of noise temperature at f_0 = 2007 Hz and V_{dc} = 0 V. Dots are experimental data and solid line data from fit functions; $P_{SLF} = 4.511 \times 10^{-8}x^2 - 8.540 \times 10^{-7}x + 3.610 \times 10^{-6}$ and $P_{SHF} = 4.843 \times 10^{-8}x^2 - 1.234 \times 10^{-6}x + 7.460 \times 10^{-6}$ where x represents the equivalent noise temperature .

[2] $P_{ac} = \frac{V_{ac}^2}{50}$ in Watt unit; in dBm unit $P_{dBm} = 10\log_{10}(10^3 P_{ac})$

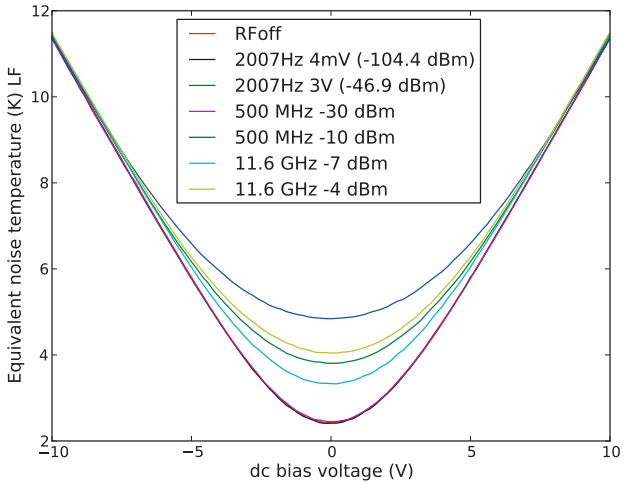

FIGURE 4.16: Variation of noise spectral density as function of V_{dc} for various V_{ac} and f_0. The temperature of the amplifier was removed from the measured noise temperature. $\alpha = 0.246 \times 10^{-3}$ V K^{-1}, $T_a = 2.82$ K and $T_a = 10.17$ K.

4.2.4 Calibration of the P_S as function of f_0

PAN was also measured as function of f_0 for two ranges of excitation frequencies: low RF; from 10 MHz to 4 GHz and high RF; from 8 GHz to 20 GHz. The V_{dc} was set to 0 V while the values of excitation power P_{ac} in dBm were taken to be -16 dBm, -13 dBm, -10 dBm and -7 dBm for low RF band and -10 dBm, - 7 dBm, - and 4 dBm. The figure 4.17 illustrates the variation of the P_S associated to the measured PAN as function of f_0. As we can notice P_S displays similar behavior for both signals in the LF or HF and its amplitude depends on f_0. This frequency dependency is caused by the presence of the cables whose effects can no longer be negligible when $f_0 \geq 10$ MHz.

4.2.5 Calibration of the P_S with P_{ac} at high frequency

Similarly procedure was used to measure to PAN vs P_{ac} from -30 dBm to 0 dBm at the frequencies where G_2 was expected to be non-zero: the sum, difference and half-difference of the central frequencies of the filters were $f_0 = 11.6$ GHz, 2.5 GHz and 1.3 GHz respectively at $V_{dc} = 0$ V; results are shown in figure 4.18. At low a.c bias, a change in frequency does not affect the amplitude of the P_S which remains almost constant. However, the situation was different when $P_{ac} \geq 20$ dBm. P_S was drastically increasing when the f_0

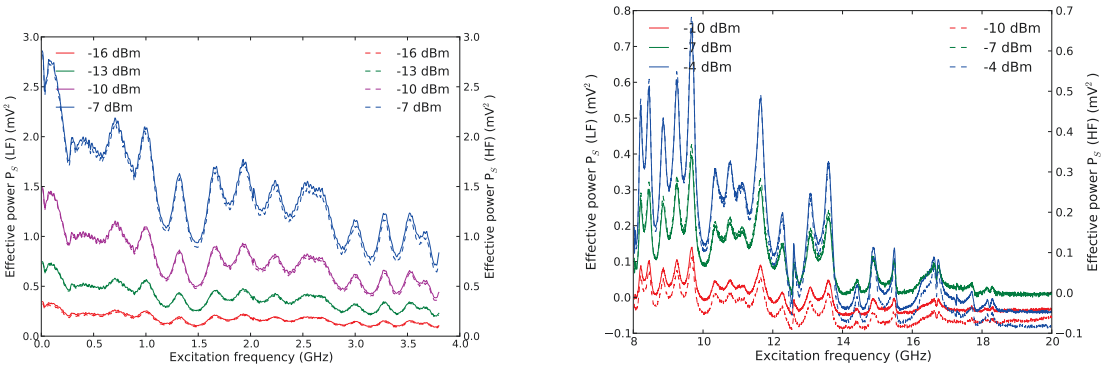

(a) 10 MHz – 4 GHz (b) 8 – 20 GHz

FIGURE 4.17: Variation of the power as function of the r.f excitation frequency f_0 at V_{dc} = 0 V for various P_{ac} in dBm. Solid line and dashed line represent signal from LF and HF respectively.

was decreasing.

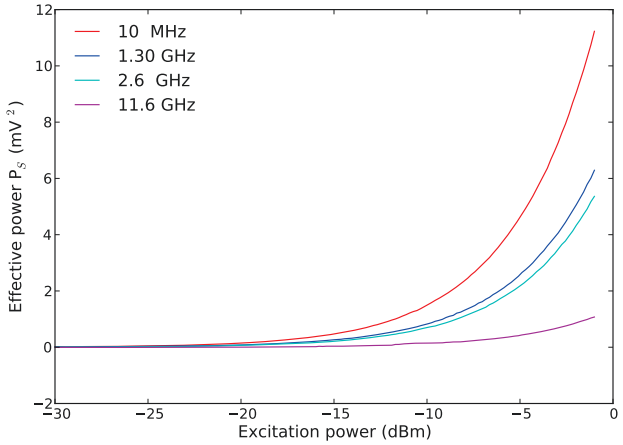

FIGURE 4.18: Calibration of effective power of the sample P_S vs r.f excitation power for various f_0 at V_{dc} = 0 V.

4.2.6 Measurement of the cross-correlation G_2

We performed the measurement G_2 using the circuit in figure 4.12 for which the principle has been previously described in the subsection 4.2.1. We investigated first the frequency dependence of G_2 at fixed d.c + a.c in order to observe peak of correlations. Later, we

fixed f_0 at the frequencies where these peaks occurred and explored how G_2 varied with the d.c bias voltage. 8192 mega samples (MS) were integrated. The digitizer integrates one sample at every 2.5 ns.

4.2.7 Measurement of fourth cumulant C_4 from the histogram

To measure a fourth cumulant from histogram methods we used the circuit in figure 4.19. The principle was the following: an r.f signal oscillating at high frequency f (4 GHz $\leq f \leq$ 8 GHz) emitted by sample was mixed with another signal at f_{os} using a nonlinear device EXA (spectrum analyzer). This in order to displace the high frequency signal f to low frequencies because to analyze f one need a very fast digitizer which we do not have. The digitizer that was on hand produced only 400 MS per second which means frequencies that are greater than 400 MHz will not be seen. After, the two signals being mixed it results at point B a superposition of signals oscillating at intermediate frequencies $f + f_{os}$ and $f - f_{os}$. The frequency $f + f_{os}$ will make worse our difficulty in analyzing high frequency so it was removed using a low pass filter. The remaining signal at point C (frequency $f - f_{os}$) given by $i(t) = \int_{-\infty}^{0} d\epsilon[i(f+\epsilon)e^{i2\pi(f-f_{os}+\epsilon)t} + i(-f-\epsilon)e^{-i2\pi(f-f_{os}-\epsilon)t}]$ was then digitized in many points each of which having 2^{14} possible levels. Via a numerical code written in python we counted the number of time a level occurs in order to compute the histograms and extract C_4 using a script following the statistic description of $C_4 = \langle i^4(t)\rangle - 3\langle i(t)^2\rangle^2$ written in python codes. Prior to that, the level of power arriving to EXA was adjusted to -26 dBm, the span xscale was set to zero. Sweep time and the resolution bandwidth RBW were set at 22.67 ms and 3 MHz.

In this study there was only one input signal, therefore we can show that the measured C_4 as in the case of autocorrelation (chapter 3) involving one frequency is given by: $C_4(f,-f,f+\Delta,-f-\Delta) \propto \langle i(f+\epsilon)i(-f-\epsilon')i(f-\epsilon'+\Delta)i(-f+\epsilon-\Delta)\rangle$.

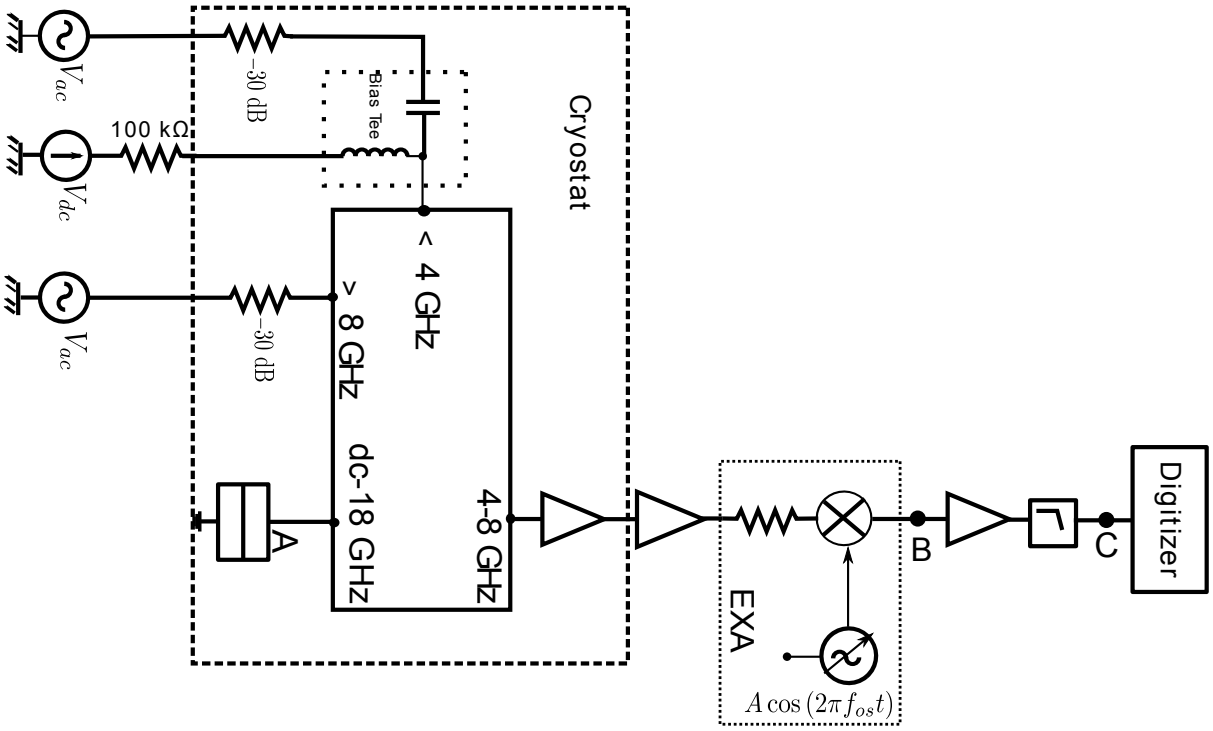

Figure 4.19: Measurement setup for the fourth cumulant of current fluctuations C_4.

Chapter 5

Results and Discussions

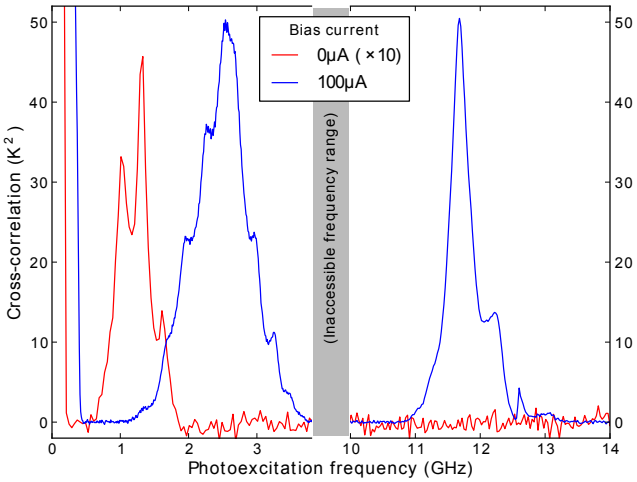

FIGURE 5.1: Variation of the cross-correlation G_2 as function of the excitation frequency at $I_{dc} = 0$ μA and $I_{dc} = 100$ μA when $P_{ac} = 16$ dBm.

5.1 Results of the measurement of G_2

5.1.1 Frequency-dependence of G_2

To investigate the frequency dependence of G_2, the power level of the r.f excitation was set to a value for which a significant change in the detection of cross-correlation was noticed. For that, we fixed $P_{ac} = -16$ dBm and measured G_2 at fixed bias voltage $V_{dc} = 0$

V or V_{dc} = 10 V for two range of the excitation frequency; d.c – 4 GHz and 8 – 15 GHz. To provide better statistics, the photo-assisted signal was digitized and averaged into 8192 MS, meaning that it took 23 s for the acquisition of one point. There was no time delay between two data acquisitions ($\tau = 0$); with these conditions it took about 2 hours to record the data illustrated in the figure 5.1.

As we can notice there are four places where G_2 is peaked. The first peak of relatively high amplitude noticed at 10 MHz for both bias voltage: $V_{dc} = 0$ V or 10 V. While, the second peak of small amplitude about 10 times smaller than the two last peaks occurred at 1.3 GHz when V_{dc} = 0 V. These two last peaks positioned at 2.6 GHz and 11.6 GHz were however obtained when V_{dc} = 10 V. These frequencies correspond to the sum, the difference and the half-difference of f_1 and f_2; $f_+ = f_2 + f_1$ = 11.6 GHz, $f_- = f_2 - f_1$ = 2.6 GHz and $f_-/2$ = 1.3 GHz respectively. It was not possible to observe a peak at $f_+/2$ = 5.8 GHz since our experimental setup (in figure 4.12) did not allow any excitation of that kind.

5.1.2 Voltage dependence of G_2

After the peaks of correlation were determined, we studied the behaviors of G_2 with respect to d.c bias voltage. This was done by setting f_0 at 10 MHz, 1.3 GHz, 2.6 GHz and 11.6 GHz and varying P_{ac}. For the first three frequencies, P_{ac} was swept step by step from -17 to -10 dBm. These powers were sufficient to produce a change in P_S as shown on the calibration (figure 4.18). For f_0 = 11.6 GHz we increased P_{ac} from -10 dBm to -1 dBm. The recorded data in arbitrary units (a.u.) depicted on the figure 5.2 could have been expressed in K^2 unit if they were normalized by the gain of the detection of noise power correlation β. The latter is the best-fit parameter of the function $\beta[T_e x \coth x + T_a]^2$ that fits the data of G_2 vs V_{dc} at V_{ac} = 0 V. This fit function is the square of the average power since when V_{ac} = 0 V, G_2 is an autocorrelation of power fluctuation; $\langle \delta P_k^2 \rangle$ which is equal to $\langle P_k \rangle^2$ plus negligible correction of fourth cumulant (see chapter 3).

We observed that G_2 displays the same behavior for both 2.6 GHz and 11.6 GHz excitation frequency. Its amplitude vanished at V_{dc} = 0 V and linearly increased with P_{ac} and V_{dc} to reach its maximum at constant value around $V_{dc} \geq 6$ V. Similar observations were found at very low excitation frequency (f_0 = 10 MHz) except the fact that the amplitude of the G_2 was non-zero at V_{dc} = 0 V but quadratically increased with P_{ac}.

In contrast, when f_0 was set to 1.3 GHz the curve of the cross-correlation shown in

figure 5.2(b) presented a maximum amplitude at V_{dc} = 0 V which increased with P_{ac} while decreasing with V_{dc}.

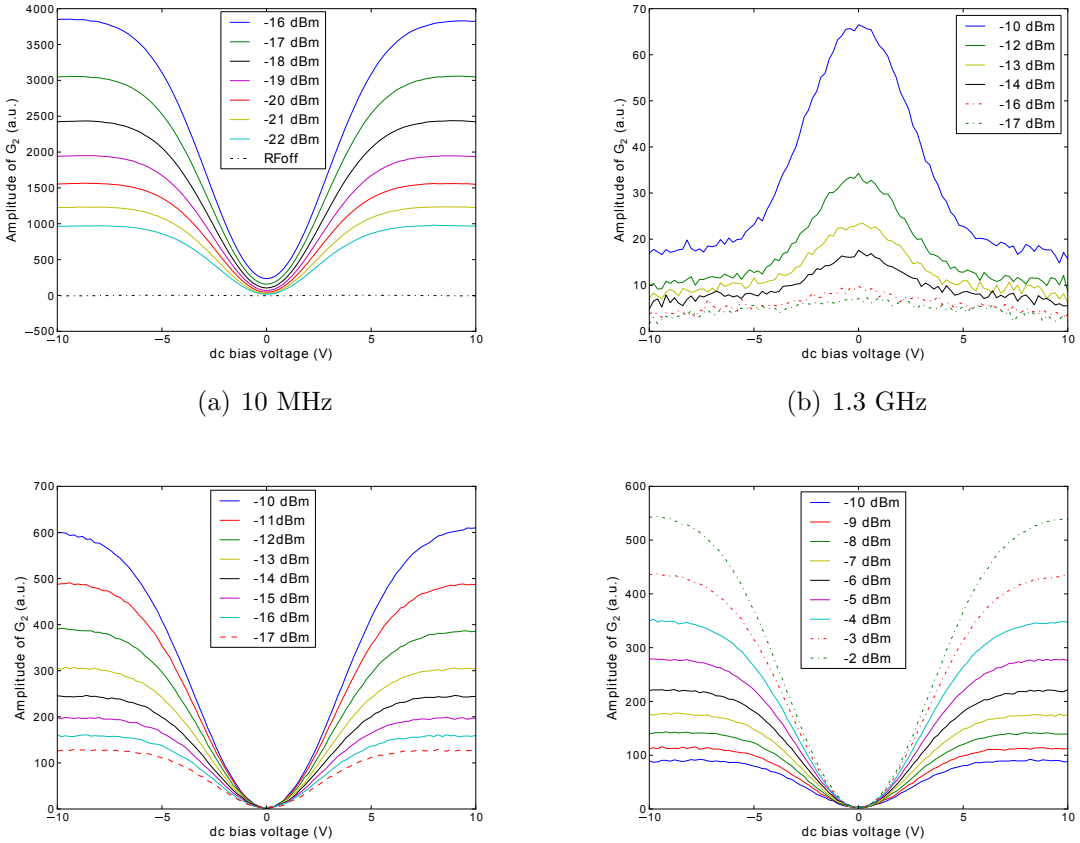

(a) 10 MHz

(b) 1.3 GHz

(c) 2.6 GHz

(d) 11.6 GHz

FIGURE 5.2: Variation of the cross-correlation G_2 as function of the dc bias voltage.

5.2 Results of the measurement of C_4

Since $G_2 = \langle \delta P_1 \delta P_2 \rangle$ leads to the fourth cumulant C_4, so should the measurement of the latter using histogram method yield to similar results. Therefore, the starting point is hereby to verify if C_4 is non-zero at 10 MHz, 1.3 GHz, 2.6 GHz and 11.6 GHz.

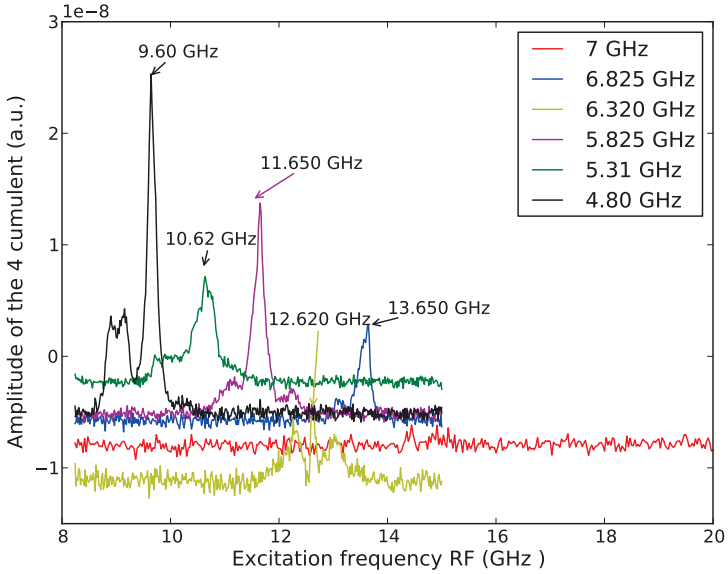

FIGURE 5.3: Frequency dependence of the fourth cumulant C_4.

5.2.1 Frequency-dependence of C_4

Figure 5.3 shows the responses of the C_4 to the excitations f_{os} and f_0. The data were obtained at $V_{dc} = 0$ V or $V_{dc} = 10$ V when the central frequencies of the spectrum analyzer f_{os} and f_0 were swept from 4.80 GHz to 7 GHz and 8 – 20 GHz respectively while P_{ac} was maintained to -16 dBm. Due to the slowness of the acquisition of data, 4096 MS were integrated.

The data revealed that the positions of the peaks of C_4 at high excitation frequency mainly depended on f_{os} and were such that $f_0 = 2 \times f_{os}$. As an example, a peak at 11.65 GHz was evidenced when $f_{os} = 5.825$ GHz. For low excitation frequencies (d.c – 4 GHz) this dependency in f_{os} was lost, since C_4 is only peaked at 10 MHz. This frequency is so small that it can be approximated to d.c frequencies.

These results can be well perceived, if we bear in mind the following image: that the two non-overlapping filters in figure 4.12 were replaced by two identical filters centered at the frequency $f_1 = f_2 = f_{os}$. Therefore, the excitation that corresponds to the sum of these central frequencies is $f_+ = 2f_{os}$ whereas their difference and half difference are reduced to $f_- = f_-/2 = 0$ or d.c. This is why the peaks at 2.6 GHz and 1.3 GHz have not been observed.

Summary. To summarize, both methods of the measurement of fourth cumulant through histogram C_4 or through cross-correlation G_2 give same results.

5.2.2 Voltage-dependence of C_4

Once the peaks of C_4 were determined, their dependence on the dc bias voltage was studied. f_0 and f_{os} were set at 10 MHz and 6 GHz respectively, the excitation power P_{ac} however varied from -24 to -19 dBm. Even for a minimum average (4046 MS), the behavior of the collected data displayed in figure 5.4(a) was similar to that of the G_2 vs V_{dc}. However, the amplitudes of the former were relatively small compared to the latter. Likewise, the curve of C_4 vs V_{dc} at high excitation frequency (*i.e.* f_0 = 11.65 GHz and f_{os} = 5.825 GHz) in figure 5.4(b) has the same characteristics as G_2 vs V_{dc} at 11.6 GHz.

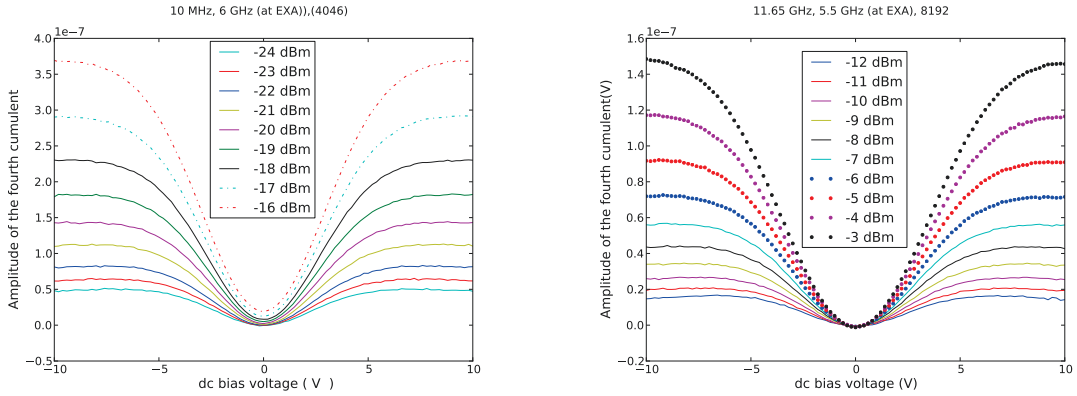

(a) (b)

FIGURE 5.4: Variation of the fourth cumulant C_4 as function V_{dc} for various excitation power P_{ac} in dBm. a.) represent data at f_0 = 10 MHz and f_{os} = 6 GHz with a minimum average of 4046 MS. b.) data at f_0 = 11.65 GHz f_{os} = 5.825 GHz with 8192 MS integrated.

5.3 Discussion: fourth cumulant

To have an intuitive understanding of the obtained results, let us model the electric current $i(t)$ as the product of a noisy signal $\zeta(t)$ and a function g(V) dependent on the amplitude of the d.c + a.c bias voltage $V = V_{dc} + V_{ac}\cos(2\pi f_0 t)$; $i(t) = \zeta(t)\mathrm{g}(V)$.

g(V) defines the width of noise dispersion hereby equal to the square root of the spectral density $\mathrm{g}(V) = \sqrt{S_{ii}(V)}$.

If V_{ac} is small enough, then g(V) can be linearly expanded as: g(V) = g(V_{dc}) + $V_{ac}\cos(2\pi f_0 t)$g′(V_{dc})+ etc. Consequently, the Fourier component of the above electric current is expressed as: $i(f) = \zeta(f)$g(V_{dc}) + V_{ac}g′(V_{dc})/2[$\zeta(f + f_0) + \zeta(f - f_0)$] + ... By setting the excitation frequency to $f_0 = f_1 + f_2$ we can show that the currents emanating from the filters 1 and 2 are given by:

$$\begin{aligned} i(f_1) &= \zeta(f_1)\mathrm{g}(V_{dc}) + V_{ac}\frac{\mathrm{g}'(V_{dc})}{2}[\zeta(f_1 + f_0) + \zeta(-f_2)] \\ i(f_2) &= \zeta(f_2)\mathrm{g}(V_{dc}) + V_{ac}\frac{\mathrm{g}'(V_{dc})}{2}[\zeta(f_2 + f_0) + \zeta(-f_1)] \end{aligned} \tag{5.1}$$

The correlator between these currents leads to $\langle i(\pm f_1)i(\pm f_2)\rangle = V_{ac}$g($V_{dc}$)g'($V_{dc}$), since $\langle\zeta(f)\zeta(f')\rangle = \delta(f + f')$. The former quantity is equal to $\frac{V_{ac}}{2}\frac{dS_{ii}}{dV}|_{V_{dc}}$ and is nothing but the correlator $X_1(f_1, f_0)$ describing noise dynamics at one harmonic frequency where $X_n(f_0, f_1) = \langle i(f_1)i(nf_0 - f_1)\rangle$ involves the *nth* harmonic frequency. In classical regime when $k_BT \gg hf$ and V_{ac} large (as in the present experiment) $X_n(f_0, f)$ corresponds to the *nth* Fourier coefficient of the oscillating spectral density $\delta S_{ii}(t) \propto (\mathrm{g}(V))^2$:

$$X_n(f_0, f) = \int_{-\pi}^{+\pi} S_{ii}(V_{dc} + V_{ac}\cos n(2\pi f_0 t))\frac{d(2\pi f_0 t)}{2\pi} \tag{5.2}$$

because [g(V)]^2 is a real, even and periodic function. So, when V_{ac} is large enough it can be expressed in Fourier series as: $(\mathrm{g}(V))^2 = \frac{a_0}{2} + \sum_{n=1}^{\infty} a_n \cos(n2\pi f_0 t)$ where $a_n = X_n(f_0, f)$ and $|\zeta(t)|^2 = 1$. From the equation 5.1 we prove that $G_2 = \langle\delta P(f_1)\delta P(f_2)\rangle$ is zero in absence of a.c excitation since each frequency is taken within independent filter. In addition, the diagram in figure 5.5 reveals that the amplitude of the correlator of the noisy signals is non vanishing at only one (*i.e.* $f = -f$).

Whenever, the a.c excitation is turned on, frequency sidebands are created around each of the central frequency (figure 5.6). In such case, G_2 is defined and is proportional to the square of Fourier coefficients such as $|X_n(f_1, nf_0 \pm f_1)|^2$ which takes non-zero values when $f_2 = nf_0 \pm f_1$. The weights functions of these correlators depend on the number of harmonics that is integrated. So, at high f_0 and small V_{ac} (2.6 GHz or 11.6 GHz $\gg \Delta f_D$ = 100 MHz) only one harmonic frequency matters. Therefore, $G_2 = a_1^2 \propto [V_{ac}\mathrm{g}(V_{dc})\mathrm{g}'(V_{dc})]^2$[1] which is non-vanishing when $V_{dc} \neq 0$ V and maximal at high d.c+a.c voltage. In contrast when f_0 is very low (10 MHz $\ll \Delta f_D$), many harmonics

[1]Note that, $V_{ac}\mathrm{g}(V_{dc})\mathrm{g}'(V_{dc}) = \frac{V_{ac}}{2}\frac{dS_{ii}}{dV}|_{V_{dc}}$

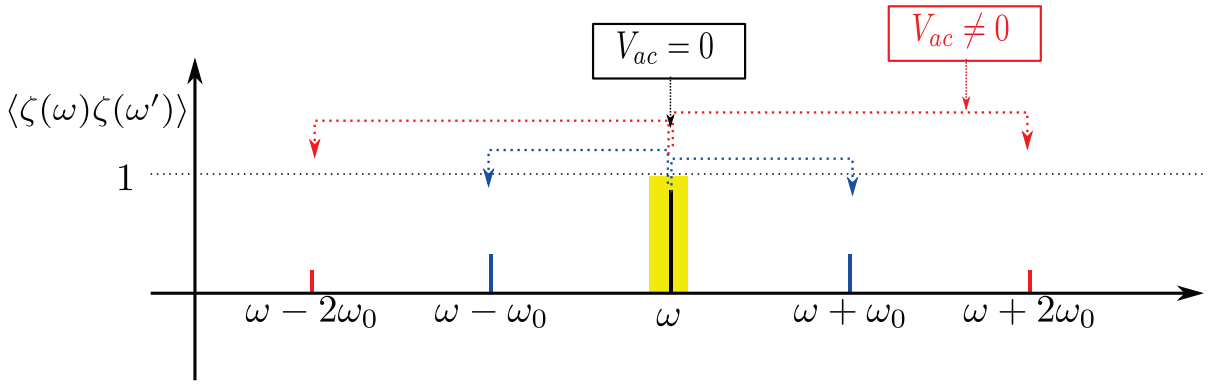

FIGURE 5.5: Formation of frequency sidebands frequencies around $\omega = 2\pi f$ in presence of a.c excitation.

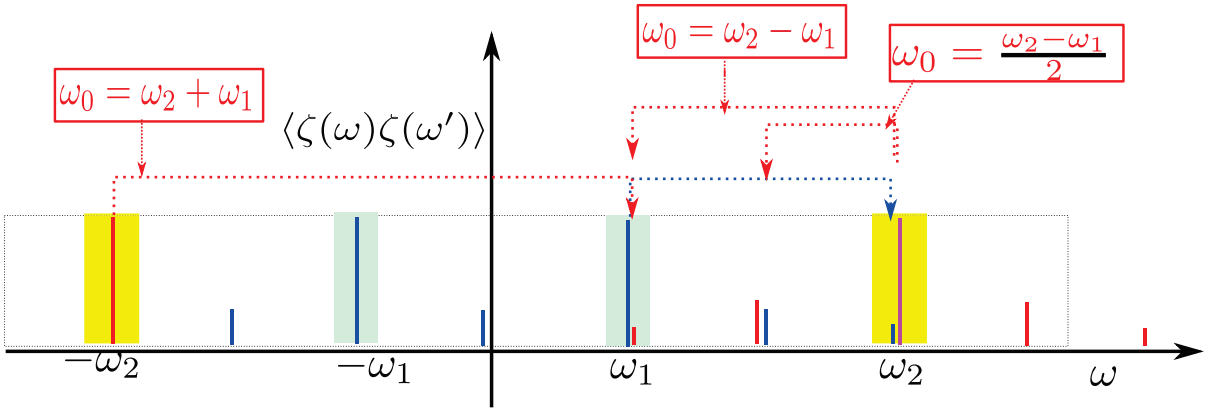

FIGURE 5.6: Formation of side band frequencies in presence of a.c excitation around $\omega_1 = 2\pi f_1$ and $\omega_2 = 2\pi f_2$ the central frequencies of the low and high bandpass filters respectively.

are involved. In such case, G_2 is given by Parseval formula associated to $[g^2(V)]^2 = [\frac{a_0}{2} + \sum_{n=1}^{\infty} a_n]^2$. For the case of two harmonics frequencies (*i.e* when $f_0 = 1.3$ GHz); $G_2 = a_2^2 = [\frac{V_{ac}^2}{4} g(V_{dc}) g''(V_{dc})]^2$[2]. The expression is maximal at $V_{dc} = 0$ V and minimal at $V_{dc} = 10$ V as shown in the figure 5.2(b); and the corresponding values are such proportional to $[V_{ac}^2 \frac{d^2 S_{ii}}{dV^2}_{V_{dc}=0}]^2$ and $[V_{ac}^2 \frac{1}{S_{ii}(V_{dc}=10\ \mathrm{V})} (\frac{dS_{ii}}{dV}_{V_{dc}=10\ \mathrm{V}})^2]^2$ respectively.[3]

[2] To obtain this quantity one need to expand the Fourier components of $i(f_1)$ and $i(f_2)$ in equation 5.1 at high order (for example second order). Then set $2f_0 = f_1 + f_2$ before computing the correlator associated to these currents.

[3] Since $g(V_{dc})g"(V_{dc}) = \frac{1}{2} \frac{d^2 S_{ii}}{dV^2}_{|V_{dc}} - \frac{1}{4 S_{ii}(V_{dc})} [\frac{dS_{ii}}{dV}_{|V_{dc}}]^2$.

Conclusion

In this dissertation, we have studied the cross-correlation between power fluctuations coming from non-overlapping filters centered at frequencies f_1 = 4.5 GHz and f_2 = 7.15 GHz and whose bandwidths are Δf_1 = 0.72 GHz and Δf_2 = 0.60 GHz respectively; $G_2 = \langle \delta P_1(t) \delta P_2(t) \rangle$ and the fourth cumulant of current noise $C_4 = \langle\langle i(t)^4 \rangle\rangle$. The purpose of these studies was to know what were the statistics of electronic transport in the presence of a.c excitation. In fact, we have noticed that even though there were many theories that highlighted the importance of the current fluctuations under microwave irradiations [3, 37], only few experiments could be found in the literature. We had therefore decided to measure the fourth cumulant of the photo-assisted noise (PAN) in a tunnel junction in order to prove its non-Gaussian repartition.

Since noise has small amplitude, it is therefore a difficult task to directly measure cumulants of order higher than two. To overcome such difficulty we established first a relation between C_4 and G_2. This relation was such that $G_2 \propto \langle i(f_1) i(-f_1+\Delta) i(f_2) i(-f_2-\Delta) \rangle = C_4(f_1, f_2, 0)$ (see chapter 3). We then designed the experimental setup to conduct the measurements of G_2 on a tunnel junction under d.c+a.c for which the experimental procedure is summarized as follows:

1. First we determined the characteristic curve of spectral density for noise and photo-assisted noise. This in order to extract the noise equivalent temperature for electron, that of the amplifier, the gain and to calibrate the effective power at sample.

2. After calibration, we searched the excitation frequencies f_0 at which G_2 presents maximum values.

3. At these frequencies we then conducted the measurement of G_2 as a function of the d.c bias voltage for various a.c bias.

According to the obtained results, G_2 is non- vanishing at specific f_0: 11.6 GHz, 2.6 GHz,

1.3 GHz and 10 MHz. In theory, these frequencies were equal to the sum, difference and half-difference of f_1 and f_2 while 10 MHz was considered as d.c.

To verify these results we measured $C_4(f, -f, 0)$ after direct conversion and digitization of photo-assisted noise at high speed. After comparing the results obtained for both measurements we noticed that G_2 and C_4 behave similarly however, the amplitudes of C_4 were very small as expected. The presence of the peaks of G_2 at specific frequencies were interpreted as the consequence of the creation of frequency sidebands at non zero a.c bias.

The same work can be done in quantum regime (*i.e.* k_B T$\ll hf$) in order to investigate photon-photon correlation.

Appendix A

Fourth cumulant of current

Following the definition in chapter, the fourth cumulant of current $C_4 = \langle\langle i(t)^4\rangle\rangle$ is a fourth moment of current from which the square dc power (or second moment of current) is subtracted

$$\langle\langle i(t)^4\rangle\rangle = \langle i(t)^4\rangle - \langle i(t)^2\rangle^2 \tag{A.1}$$

If at a given time t the expression of the current $i(t)$ in terms of its Fourier componenent $i(f)$ is given by:

$$i(t) = \int_0^\infty \mathrm{d}f[e^{i2\pi ft}i(f) + e^{-i2\pi ft}i(-f)] \tag{A.2}$$

Then, the associated instantaneous power per unit resistance $P(t) = i(t)^2$ is such that:

$$P(t) = \int_0^\infty df_1 df_2[e^{i2\pi(f_2-f_1)t}i(f_1)i(-f_2) + e^{-i2\pi(f_2-f_1)t}i(-f_1)i(f_2) + ...] \tag{A.3}$$

Where f_1 and f_2 are any positive frequencies. This power when time averaged gives $\langle i(t)^2\rangle = 2\delta f S(f)$. Using equation A.3 one compute the fourth moment of current:

$$\begin{aligned}\langle i(t)^4\rangle \;=\; & 2\int_0^\infty df_1 df_2 df_3 df_4[\delta(f_2 - f_1 + f_3 - f_4)\langle i(-f_1)i(f_2)i(-f_3)i(f_4)\rangle + \\ & \delta(-f_2 + f_1 + f_3 - f_4)\langle i(f_1)i(-f_2)i(f_3)i(-f_4)\rangle + ...]\end{aligned} \tag{A.4}$$

Here f_1 and f_2 are taken in the same filter of bandwidth Δf and f_3 and f_4 are in an other filter $\Delta f'$. (...) stand for higher terms involving higher frequencies, these terms are

neglected at low frequencies. The equation A.4 leads to non-zero values only when:

$$(-f_2+f_1+f_3-f_4) = 0 \Rightarrow \begin{cases} f_2 - f_1 = 0 & \text{and} \quad f_3 - f_4 = 0 \quad \text{i.e. dc which are removed} \\ f_2 - f_1 = \Delta & \text{and} \quad f_3 - f_4 = -\Delta \end{cases} \tag{A.5}$$

It follows that:

$$C_4 = 4 \int_0^{\Delta f} \int_0^{\Delta f'} df_1 df_3 \langle i(f_1) i(-\Delta - f_1) i(-f_3) i(\Delta + f_3) \rangle. \tag{A.6}$$

Appendix B

Detailed procedures

B.1 Cooling procedures

In order to cool properly the temperatures of dewar down to the one of the liquid Helium 4, ^{4}LHe (4.2 K); an important condition much be filled. The pressure inside dewar must be below 5×10^{-5} Tor. For that, we pumped for about 2 hours the guard vacuum using a turbo pump to evacuate the nitrogen atoms and reduce the atmospheric pressure. After the gas molecules were removed and the desired pressure established, we pre-cooled the system by filling it with liquid nitrogen LN_2 and waited until equilibrium temperature was reached 77 K[1]. This being done, we removed LN_2 from the He container while keeping the N_2 container fully filled before starting the transfer of ^{4}LHe. We transfered ^{4}LHe and let the temperature of the system re-equilibrate to 4.2 K.

B.2 Optimization of the signal to noise ratio (SNR)

Since almost all commercial devices have a non-zero resistance 50 Ω which is greater than R_S = 22.8 Ω, therefore during the generation or detection of the electric signal emitted by the sample, an amount of this signal will be lost due to reflections. To reduce these losses and the effects of the undesired noise produce by the amplifier the experiment has to be carried out at the operating point of the amplifier. This point is such that the gains of the amplifiers and the SNR give maximal values (see figure B.1), *i.e.* T_a minimal or approaching to T_e. For that, several filters and circuit have been tested. The best filters

[1]The pre-cool was a very important step to avoid many losses in liquid He due to evaporation ($300K \gg 4.2K$)

were those presenting non-overlapping bandwidth as shown in table **??**. The subsections B.2.1 and B.2.2 detailed how these filters and components of each circuits were tested in order to choose the best one.

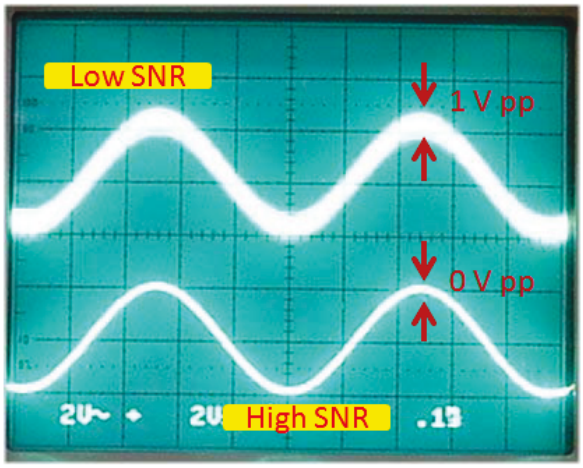

FIGURE *B.1:* Schematic representation the SNR seen on the oscilloscope. The top diagram illustrates a noisy signal with high T_a and low diagram is a parfait signal $T_a \approx 0$.

Tests	Filters & bandwidth GHz	T_e K	T_a K	gain α V K^{-1}
1	4.2–4.7	4.83	17.29	1.18×10^{-3}
	5.6–7	4.661	22.84	1.09×10^{-3}
2	4.2–4.7	4.15	14.74	0.82×10^{-3}
	5.6–7	3.93	15.67	1.09×10^{-3}
3	LF= 3.2–5.2	4.15	7.25	1.15×10^{-3}
	HF= 6.9–7.7	4.22	12. 365	0.282×10^{-3}

TABLEAU *B.1:* List of the parameters for the best fit function for the curve of NSD vs V_{dc}. LF stand to low bandpass filter (VBF–4440$^+$ + VLF-5500) and HF is high bandpass filter (VHF–6010$^+$ + VHF–6010$^+$).

B.2.1 Tested materials

In early experiments (from 2011/12/12 to 2012/05/27), we have expended most of our time in testing almost all devices on hand. The table B.2 presents the list of materials used in this study. Most of these materials such as the filters were tested with a network analyzer (PNA-L), except for the characterization of the operating point or gain of the

amplifier for which we used a spectrum analyzer (EXA). To determine the bandwidth of a filter band, a signal was sent to one of its port and the frequency-dependence transmission to the other port was measured. Prior to that, the instrument set up of the PNA-L was calibrated in order to cancel the effects of the r.f frequency due to the of coaxial cables on the probing. The results obtained were comparable to commercial bandwidth.

	Characteristics	
Materials	Serial number	Bandwidth
Cryogenic amplifier		4–8 GHz
Amplifier		0.1–12 GHz
Bias Tee		
Duplexer 2	K&L 11SZ10–0087	
Duplexer 3	K&L 11SZ10–0086	
Dc sources	Yokogawa GS200	
Ac sources: low RF	Lock In amplifier SR30 DSP	DC–4.05 GHz
Ac sources: high RF	E8257D	250 KHz–40 GHz
Diodes	DTM180AA	100 MHz
Filter 1	VBF–4440$^+$	4.2–4.7 GHz
Filter 2	VBFZ–6260–S$^+$	5.6–7 GHz
Filter 3	VLF–5500$^+$	DC – 5.5 GHz
Filter 4	VBF–7200$^+$	7.1 –7.3 GHz
Filter 5	VHF–6010$^+$	6.3 –15 GHz
Filter Low (LF)	VBF–4440$^+$ + VLF–5500$^+$	3.2–5.2 GHz
Filter High (HF)	VHF–6010$^+$ + VHF–6010$^+$	6.9–7.7 Ghz

TABLEAU *B.2:* List of materials used to test and design the experiment circuit and their characteristics.

B.2.2 Choice of the best circuit

To measure a fourth cumulant using cross-correlation, not only the independent bandpass filters matter, but the environment of sample must also be carefully taken into account since the correlator G_2 involves four quantities (current) of small amplitudes which can easily be perturbated by the electromagnetic RF (noise). To decrease this electromagnetic noise, we added filters, attenuators, mini-amplifiers, etc... to the circuit (figure 4.3). We have design three circuits, in all them the sample was cooled inside the cryostat of model HDL-10 Helium at 4.2 K.

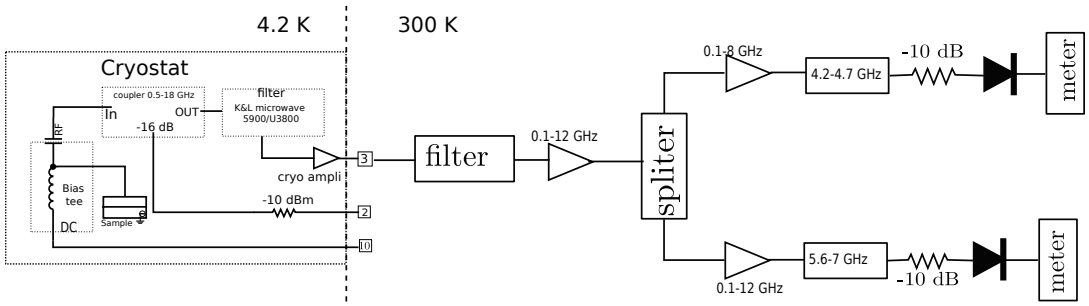

FIGURE B.2: Circuit 1 design for testing the filters: VBF–4440$^+$ (4.2–4.7 GHz) and VBFZ–6260–S$^+$ (5.6–7 GHz), with a cryostat containing a coupler.

At first, we tested the filter 1 and filter 2 (in table B.2) using a circuit 1 (ref figure B.2) containing two regions. A cooled region inside which the sample, the cryogenic amplifier, the bias Tee, the coupler, -10 dB attenuator and K&L microwave 5500/U3800 filter were mounted. This region was connected through the d.c port (10), the a.c ports (2 and 4) and output canal (3) to a hot region (300 K) containing all the voltage sources, measurement devices and the filters to be tested. With this configuration, the a.c current generated by the biased sample was first filtered and amplified inside the cooled region, then further amplified and filtered outside before being split to pass into two branches each holding a bandpass filter; filter 1 (4.2–4.7 GHz) on branch 1 and filter 2 (5.6 – 7 GHz) on branch 2 and a diode (DTM180AA). For the second test, we used the measurement circuit 2 (not depicted here) for which the coupler in circuit 1 was replaced with a two combining duplexer: K&L 11SZ10–0087 and K&L 11SZ10–0086. Later on, we conducted the third test in a circuit 3 in which the filter 1 and filter 2 in circuit 2 were replaced by two combination of bandpass filters: LF = VBF–4440$^+$ + VLF–5500$^+$ and HF = VHF–6010$^+$ + VHF–6010$^+$. The measured data for the NSD and their corresponding T_e, T_a and α for the three circuits are shown in table **??**.

We note that the T_e of electrons emanating from both branches of each circuit is approximately equal to the temperature of the cryostat T = 4.2 K. The latter is however 4 times smaller than the T_e for the cryogenic amplifier (except for filter LF) whose most remarkable values were obtained in the presence of coupler, in contrast to the diplexer. Considering the results, the circuit 3 is expected to be the most adapted for the measurement of the noise power correlation not because we gained more signal but because the noise temperature of the amplifier was not too distant from that of the electrons and the SNR was thus maximized.

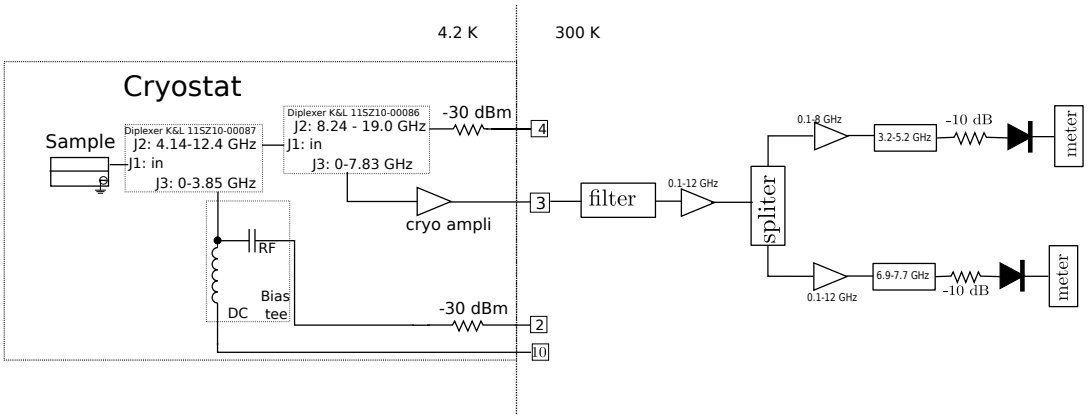

Figure B.3: Circuit 3 for testing the combining filters: VLF–5500$^+$ + VBF–4440$^+$ (3.2–4.7 GHz) and VBF–7200$^+$ + VHF–6010$^+$ (6.9–7.7 GHz). Here cryostat contains a two diplexers.

Bibliography

[1] Kim, P. T. *The Canadian Journal of Statistics / La Revue Canadienne de Statistique* **17**(3), pp. 285–299 (1989).

[2] Loudon, R. *The Quantum Theory of Light*. Oxford University Press, third edition, (2000).

[3] Lesovik, G. B. and Levitov, L. S. *Phys. Rev. Lett.* **72**, 538–541 Jan (1994).

[4] Levitov, L. S. and Reznikov, M. *Phys. Rev. B* **70**, 115305 Sep (2004).

[5] Landauer, R. *Nature* **392**, 658–659 (1998).

[6] Nazorov, Y. V., editor. *Quantum Noise in Mesoscopic Physics*, volume 97 of *II. Mathematics, Physics and Chemistry*. Kluwer Academic Publishers, (2002).

[7] Bouchiat, H., Gefen, Y., Guéron, S., Montambaux, G., and Dalibard, J., editors. *nanophysics: coherence and transport*. Elsevier, (2005).

[8] Brown, R. H. and Twiss, R. Q. *Proceedings of the Royal Society of London. Series A, Mathematical and Physical Sciences* **242**(1230), pp. 300–324 (1957).

[9] Goldberger, M. L., Lewis, H. W., and Watson, K. M. *Phys. Rev.* **142**(1), 25–32 (1966).

[10] Büttiker, M. *Phys. Rev. Lett.* **68**, 843–846 Feb (1992).

[11] Blanter, Y. and Büttiker, M. *Physics Reports* **336**(1), 1–166 (2000).

[12] Schoelkopf, R. J., Kozhevnikov, A. A., Prober, D. E., and Rooks, M. J. *Phys. Rev. Lett.* **80**, 2437–2440 Mar (1998).

[13] Forgues, J.-C., Sane, F. B., Blanchard, S., Spietz, L., Lupien, C., and Reulet, B. *Scientific Reports* **3**, 2869 Sep (2013).

[14] Gasse, G., Lupien, C., and Reulet, B. *Phys. Rev. Lett.* **111**, 136601 Sep (2013).

[15] Viljas, J. and Cuevas, J. *Physical Review B* **75**(7), 075406 February (2007).

[16] Gabelli, J. and Reulet, B. (2007).

[17] Zakka-Bajjani, E., Dufouleur, J., Coulombel, N., Roche, P., Glattli, D. C., and Portier, F. *Phys. Rev. Lett.* **104**, 206802 May (2010).

[18] Bendat, J. S. and Piersol, A. G. *Engireering Applications of Correlation and Spectral Analysis*. John Wiley & Sons, Inc, (1980).

[19] Vasilescu, G. *Bruits et Signaux Parasites*. DUNOD, Paris, (1999).

[20] Bendat, J. S. and Piersol, A. G. *Random data: Analysis and measurement procedures*. Wiley-Interscience, (1971).

[21] A., R. W. *Design of Low–Noise Transistor Input Circuits*. New York: Hayden, (1964).

[22] Landauer, R. *Physica B: Condensed Matter* **227**(1-4), 156–160 (1996).

[23] Kumar, A., Saminadayar, L., Glattli, D. C., Jin, Y., and Etienne, B. *Phys. Rev. Lett.* **76**, 2778–2781 Apr (1996).

[24] Büttiker, M. *Phys. Rev. Lett.* **65**, 2901–2904 Dec (1990).

[25] Schoelkopf, R., Burke, P., Kozhevnikov, a., Prober, D., and Rooks, M. *Physical Review Letters* **78**(17), 3370–3373 April (1997).

[26] Saminadayar, L., Glattli, D. C., Jin, Y., and Etienne, B. *Phys. Rev. Lett.* **79**, 2526–2529 Sep (1997).

[27] Gabelli, J. and Reulet, B. *Journal of Statistical Mechanics: Theory and Experiment* **2009**(01), P01049 (2009).

[28] Reulet, B. and Prober, D. *Physical Review Letters* **95**(6), 066602 August (2005).

[29] Gabelli, J. and Reulet, B. *Physical Review Letters* **100**(2), 026601 January (2008).

[30] Jacques, V. *Ann. Phys. Fr.* **32**(6), 1–136 (2007).

[31] Dayem, A. H. and Martin, R. J. *Phys. Rev. Lett.* **8**, 246–248 Mar (1962).

[32] Landauer, R. *IBM Journal of Research and Development* **1**(3), 223–231 (1957).

[33] Lee, H. and Levitov, L. S. *Phys. Rev. B* **53**, 7383–7391 Mar (1996).

[34] Nyquist, N. *Phys. Rev.* **32** (1928).

[35] Tien, P. K. and Gordon, J. P. *Phys. Rev.* **129** (1963).

[36] Spietz, L., Lehnert, K. W., Siddiqi, I., and Schoelkopf, R. J. *Science* **300**(5627), 1929–1932 (2003).

[37] Sindel, M., Hofstetter, W., von Delft, J., and Kindermann, M. *Phys. Rev. Lett.* **94**, 196602 May (2005).